Evidence for Regional-Scale, Pluton-Driven, High-Grade Metamorphism in the Archaean Minto Block, Northern Superior Province, Canada

Jean H. Bédard

Geological Survey of Canada, GSC-Québec, CP 7500, Sainte-Foy, Québec G1V 4C7, Canada
(*e-mail: jbedard@rncan.gc.ca*)

ABSTRACT

The Archaean Minto Block of the Superior Province is dominated by foliated tonalite, trondhjemite, granite, granodiorite, enderbite, and clinopyroxene- or orthopyroxene-bearing hornblende-tonalite; most partly retain igneous microtextures. Outcrop-scale structures such as melt-filled shear zones and deformed intraplutonic dikes imply that deformation was synmagmatic. Compositions of epidote (pistachite 25–30), garnet, and muscovite (FeO^* 4.5–6 wt%, TiO_2 0.5–1.7 wt%) are typically igneous. Epidote commonly has allanite cores, some with igneous growth zoning. Epidote, muscovite, and allanite are embayed where they touch the quartzofeldspathic matrix. These embayments are interpreted as magmatic resorption structures. Biotite and muscovite armor epidote and allanite against resorption. Since epidote and muscovite stabilities are pressure dependent, these resorption structures suggest that magmas ascended as crystal-charged mushes. The Al-in-hornblende geobarometer yields regionally uniform pressures (4–6.4 kbar), with tonalite from the eastern Minto Block yielding pressures about 1 kbar higher than elsewhere. The plagioclase-hornblende thermometer yields similar temperatures for tonalite-trondhjemite (666°–793°C at 5 kbar) and pyroxene-tonalite (723°–783°C) but higher temperatures (801°–948°C) for hornblende-bearing enderbite. Reintegrated preexsolution antiperthite grains plotted on a 5 kbar solvus yield 550°–870°C for tonalite-trondhjemite and 810°–1045°C for enderbite. Comparison of geothermobarometric calculations with published tonalite phase equilibria suggests near-solidus deformation. Thus, petrographic, mineralogic, field, and microstructural data are inconsistent with tectonometamorphic models requiring transposition and complete recrystallization of preexisting fabrics during regional orogenesis. Amphibolite-grade supercrustal rocks are associated with tonalite-trondhjemite or granite-granodiorite plutons, while granulite-grade belts are associated with enderbite and clinopyroxene- or orthopyroxene-bearing tonalite. This dichotomy suggests that metamorphism of supercrustal rocks reflects localized equilibration with adjacent plutons rather than orogenesis.

Introduction

Deciphering the pressure-temperature evolution of a crustal segment is a prerequisite to understanding its tectonometamorphic history. Supercrustal rocks in Archean granite-greenstone terrains occur as coherent belts, generally of low metamorphic grade, and as small higher-grade slivers embedded in plutonic rocks. Thermobarometric calculations are commonly applied to the metavolcanic and metasedimentary rocks because many well-calibrated geothermometers and geobarometers are available for metapelitic and metabasic assemblages. In contrast, the *PT* history of the plutonic component of these terrains is less clearly understood, and the "gneissic" appearance of many plutons has led to the common use of terms appropriate to metamorphic processes in an orogenic context, such as amphibolite- or granulite-grade assemblages, orthogneiss, diatexite, and so forth.

The Minto Block (fig. 1), the largest plutonic-dominated Archean terrane of the Superior Province (Card 1990), is an ideal place to discriminate between an igneous and a metamorphic origin for mineral assemblages and fabrics in the plutonic rocks and to contrast thermobarometric results from supercrustal and adjacent plutonic rocks in order to constrain the links between tectonism, metamorphism, and plutonism. This article presents field, textural and mineralogical observations

Manuscript received December 13, 2001; accepted June 12, 2002.

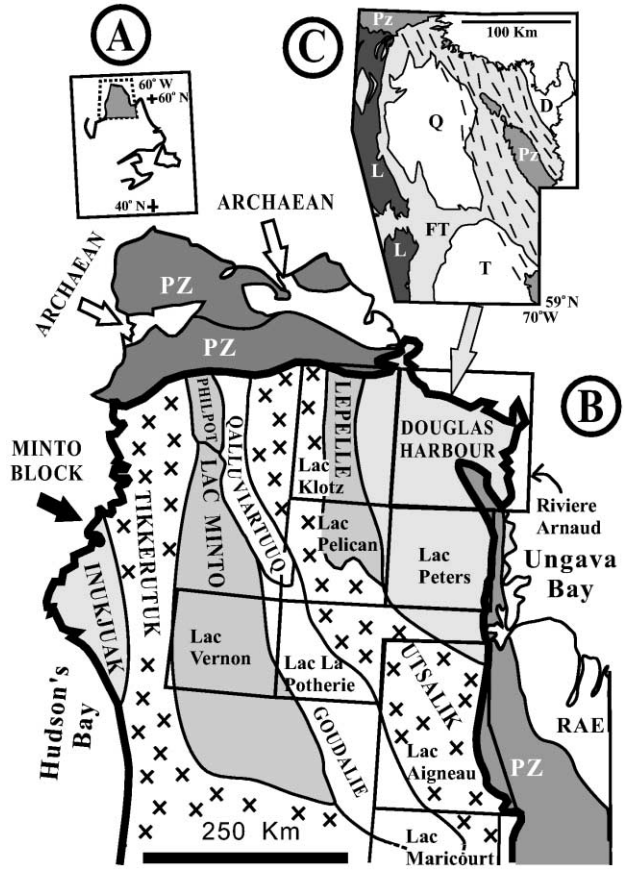

Figure 1. Simplified geological map of northern Quebec, showing the domain boundaries from Percival and Skulski (2000) and the locations of the map sheets named in the text. Inset *A* shows the location of map *B*, while inset *C* (adapted from Bédard et al. 2003) shows a detail of the Douglas Harbour domain from the Lac Peters, Pélican, Klotz, and Rivière Arnaud map sheets. Bold line in *B* surrounds Minto Block. Dashes in *C* mark areas strongly affected by Proterozoic deformation. *FT* = Faribault Thury complex, *T* = Troie complex, *Q* = Quimussinguat complex, *L* = Lepelle complex, *PZ* = Proterozoic rocks. *D* = Diana complex, an Archaean terrane accreted to the Minto Block in the Proterozoic.

and data, and thermobarometric calculations for plutonic and supercrustal rocks from the Minto Block.

Summary of Previous Work

John Percival and his coworkers (see references in Percival et al. 2001) first subdivided the Minto into lithotectonic domains (fig. 1). Tonalite and trondhjemite with embedded supercrustal belts from the Goudalie and Douglas Harbour domains are the oldest rocks of the Minto Block (3–2.87 Ga; Stern et al. 1994; Percival et al. 1997, 2001; Madore et al. 1999; Percival and Skulski 2000). The juvenile isotopic signatures of Qalluviartuuq belt lavas (2.84–2.83 Ga) were considered evidence for an intraoceanic arc setting (Skulski et al. 1996). A 2.81-Ga shear zone in the Qalluviartuuq belt was interpreted as an intraoceanic accretionary thrust (D1, Percival and Skulski 2000). However, since analogous D1 structures are younger in the Vizien belt (<2.718 Ga), D1 cannot correspond to a single regional event (Percival and Skulski 2000).

Calc-alkaline volcanics (ca. 2.76 Ga) of the Kogaluc belt (Lac Minto domain) show isotopic evidence of crustal contamination (Skulski et al. 1996); and younger (<2.748 Ga), unconformable greywacke and iron formations contain ancient detritus (Percival et al. 1995). Quartzites and ultramafic lavas in the Faribault belt (Douglas Harbour domain) were interpreted as belonging to an ancient platformal cover (Percival et al. 1997). From these relationships, Percival et al. (2001) proposed that oceanic and continental terranes docked at about 2.77 Ga to create a composite cratonic basement, with successor arc magmatism at 2.77–2.76 Ga (Kogaluc belt, Lac Minto domain), followed by a continental overlap sequence (<2.748 Ga) linked to intra-arc extension by Skulski et al. (1994).

This older composite basement was intruded by voluminous granodiorite and granite (subordinate tonalite, enderbite, pyroxene tonalite, and mafic intrusions) of the Leaf River Suite (2.73–2.72 Ga; Percival et al. 1994; Stern et al. 1994), which constitutes most of the Lac Minto and Utsalik domains. In the Vizien belt (Goudalie domain), calc-alkaline andesitic to rhyodacitic lavas have ages and geochemical signatures that overlap those of Leaf River Suite plutons (Skulski and Percival 1996), suggesting a cogenetic relationship and supporting assembly of the Lac Minto, Goudalie, and Utsalik domains before 2.73 Ga (Percival et al. 2001). The calc-alkaline Leaf River Suite has Nd-isotopic signatures and relict zircon cores, indicating recycling of older continental crust, and were interpreted as Andean-type continental arcs (Percival et al. 1994; Stern et al. 1994). The great areal extent of synchronous magmatism and heterogeneous Nd-isotopic signatures were explained in terms of two subduction zones simultaneously active on opposite sides of the protocraton (Percival et al. 2001).

Lin et al. (1996) proposed that collision and amalgamation of the Lac Minto, Goudalie, and Utsalik arcs generated the dominant NNW foliation of a regionally distributed tectonometamorphic episode (D2). Subsequently, Percival and Skulski (2000) dated a D2 fabric at 2.693–2.675 Ga and reinter-

preted D2 as an overprint related to overthrusting of the 2.71–2.7-Ga Tikkerutuk continental arc onto the amalgamated Lac Minto + Goudalie + Utsalik + Douglas Harbour terrane. They further proposed that deformation and metamorphism to the amphibolite and granulite facies in supercrustal belts of the west-central Minto Block result from this crustal-thickening event (D2), as do transposition and recrystallization of all older fabrics into the dominant NNW grain and production of crustally derived plutons and diatexites (2.696–2.693 Ga). Finally, there is a series of less penetrative deformation events (D3–D5; Lin et al. 1996; Percival and Skulski 2000) and late- to posttectonic granitoid and syenite intrusions (2.690–2.675 Ga; Stern et al. 1994; Skulski et al. 1996; Percival and Skulski 2000).

Samples and Methodology

Samples are from the Goudalie, Lac Minto, Utsalik, Lepelle, and Douglas Harbour domains (fig. 1*B*). General descriptions of most domains are in Percival et al. (1992, 1994, 2001). Sampling was focused on tonalite, trondhjemite, clinopyroxene-tonalite, and enderbite. Most of the rocks studied here formed roughly synchronously with the main Leaf River Suite event (~2.73 Ga, see below). The Douglas Harbour domain was poorly known prior to mapping by the Ministère des Ressources Naturelles du Québec (Madore et al. 1999, 2001; Madore and Larbi 2000; Leclair et al. 2001; Cadieux et al. 2002; Bédard et al. 2003), which defined three Archean lithotectonic complexes (fig. 1*C*). The Faribault-Thury complex is dominated by hornblende-biotite tonalite and biotite trondhjemite (TT series) and contains numerous amphibolite-grade supercrustal belts. The western part of the complex is older than the eastern part (2.88–2.86 Ga vs. 2.81–2.77 Ga; Madore et al. 1999; Percival et al. 2001). The Troie and Qimussinguat complexes are large domiform 2.74–2.73-Ga enderbite (E series) masses (~100 km diameter) at the core of the Faribault-Thury complex (Madore et al. 1999; Percival et al. 2001). They contain granulite-grade supercrustal belts and are cut by late- to post-kinematic porphyritic quartz monzonite (MZ series, 2.697 Ga) and associated gabbro-norite and diorite of shoshonitic affinity (Madore et al. 1999). All rocks of shoshonitic affinity discussed in this article are from the Troie complex. The N-NNW grain of the Minto Block also characterizes the Douglas Harbour domain.

Mineral-chemical data were generated at Laval University on a 5-spectrometer, wavelength dispersive Cameca SX-100, calibrated against natural and synthetic standards and reduced using the internal software. Acceleration potential for most phases was 15 kV with a 20-nA current and a 10-s count time, with longer counts (15–20 s) for minor and trace elements. Tables A1–A4 are in *The Journal of Geology* data depository and are available upon request. The data set and sample coordinates are available from the author.

Lithological Assemblages and Petrography

The Tonalite-Trondhjemite (TT) Series. Plutons of the TT series occur throughout the Minto Block but are most abundant in the Goudalie and Douglas Harbour domains. There is no apparent textural or mineralogical difference between older (2.77–2.86 Ga) or younger (2.73–2.72 Ga) rocks, so all are described together. The series is dominated by biotite + hornblende-tonalite and biotite-trondhjemite, with subordinate diorite and hornblende gabbro. Tonalite and trondhjemite can be interlayered on centimeter to meter scales, with scattered, deformed enclaves of metabasite, calc-silicate, paragneiss, pyroxenite, and so forth. Melanosome sheaths separating tonalite from trondhjemite are notably absent, suggesting that these are not migmatitic complexes. Trondhjemite may fill strain shadows near enclaves and occupy shear zones in tonalite (fig. 2*A*). Trondhjemitic breccia complexes contain tonalitic to dioritic enclaves in various states of transition from angular blocks to elongate schlieren. Intratonalite dikes (1–3 m) contain incompletely mingled melatonalite and trondhjemite (fig. 2*B*). These features suggest that most TT suite rocks were not fully crystallized during deformation, so that magmatism was typically synkinematic. Domains of layered tonalite-trondhjemite alternate on a 1–15-km scale with larger, discrete intrusions of homogeneous trondhjemite or tonalite (Simard et al. 2001), though, even here, the fabric is nearly penetrative, with mafic minerals being concentrated into elongate, schlieren, typically of centimetric thickness (fig. 2*C*).

Mineral foliation is defined by the preferential orientation of mafic mineral aggregates (fig. 2*A*, 2*C*), is generally parallel to layering, and dips steeply. Planar fabrics generally strike N to NNW (i.e., D2), except in the noses of kilometer-scale fold closures (Bédard et al. 2003). Mineral lineations commonly plunge subvertically, and L-tectonites are locally prominent (Madore et al. 1999, 2001). Later Archean overprints (D3–D5) reorient the early foliation along major shear zones (Leclair et al. 2001; Parent et al. 2002). Proterozoic orogenesis

affects the easternmost Minto Block (fig. 1*C*), with preservation of Archean fabrics between major deformation corridors (Madore and Larbi 2000).

Tonalite typically has 10%–30% ferromagnesian minerals (mostly hornblende + biotite). Euhedral, commonly antiperthitic plagioclase phenocrysts (<20%; 1–5 cm) are uncommon. Hornblende or biotite grains in a thin section generally do not share optic axes, suggesting substantial grain rotation or translation during deformation (fig. 3*A*). Large, twinned, subhedral hornblende grains may represent phenocrysts. Trains of touching anhedral hornblende grains aligned parallel to the lineation show limited relative rotation of crystallographic axes and may be dislocated phenocrysts affected by dynamic recrystallization (e.g., Kruse and Stünitz 1999). Biotite commonly rims hornblende. Muscovite is common and can be the dominant mica. Muscovite intergrown with biotite is faceted, while muscovite in contact with quartz or plagioclase has irregular, wormy terminations (fig. 3*B*). Minor titanite granules and apatite prisms are ubiquitous (fig. 3*A*). Magnetite and ilmenite (1%–4%) form coarse lamellar intergrowths or occur as discrete grains. Ilmenite may be rimmed by titanite or hematite. Quartz is interstitial in weakly deformed rocks. Interstitial alkali feldspar typically constitutes <5% in Douglas Harbour TT rocks but is slightly more abundant in other domains (8%–12%). Typically, feldspar-feldspar grain boundaries are serrated, with common rotational subgrains (fig. 3*F*).

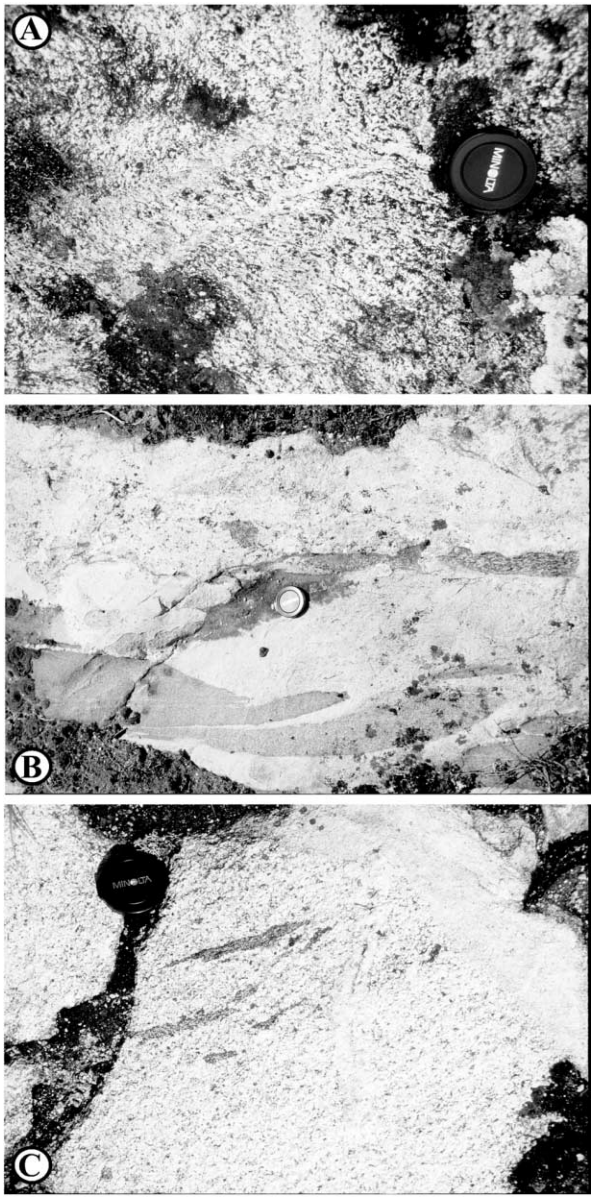

Figure 2. Field photographs, Lac Maricourt area. Lens cap is 55 mm wide. *A*, Trondhjemite segregation filling a small shear zone in a tonalite. *B*, Lower part shows an intraplutonic dike filled with mingled melatonalite and trondhjemite. Note the lobate magma/magma interfaces. The contact between the dike and the host trondhjemite (upper part of photo) is sharp and shallowly discordant to the mineral foliation in the host. *C*, Typical schlieren layering in trondhjemite. A late granite dike cuts the foliation in the upper right.

Pale green prismatic epidote (0.5%–5%) is extremely common in tonalite. In less deformed rocks, it is euhedral when embedded in biotite or muscovite (fig. 3*B*), but it is embayed and exhibits wormy textures against quartz or feldspar (figs. 3*A*–3*D*, 4). The embayments truncate concentric growth zoning. Allanite cores to epidote grains are common (figs. 3*B*–3*D*, 4, 5*C*). Allanite is generally metamict but may preserve fine, concentric lamellar growth zoning (fig. 5*A*) or exhibit complex internal discontinuities and zones that probably reflect multiple growth/dissolution events (fig. 5*A*, 5*C*). The development of very fine-grained Th- and rare-earth minerals at dissolution surfaces could reflect the low solubility of these elements in felsic melts (Rapp and Watson 1986) and/or an incongruent dissolution mechanism (Wolf and London 1995). The allanite and pale-green epidote grains typifying Minto Block tonalites are interpreted to be igneous phases. In contrast with most occurrences (Zen and Hammarstrom 1984), igneous epidote in the Minto Block rarely contains hornblende inclusions. With progressive deformation, the more competent epidote breaks up into domino structures and microboudins (cf. Stünitz and Tullis 2001) and eventually evolves into slivers enclosed within biotite or muscovite fish.

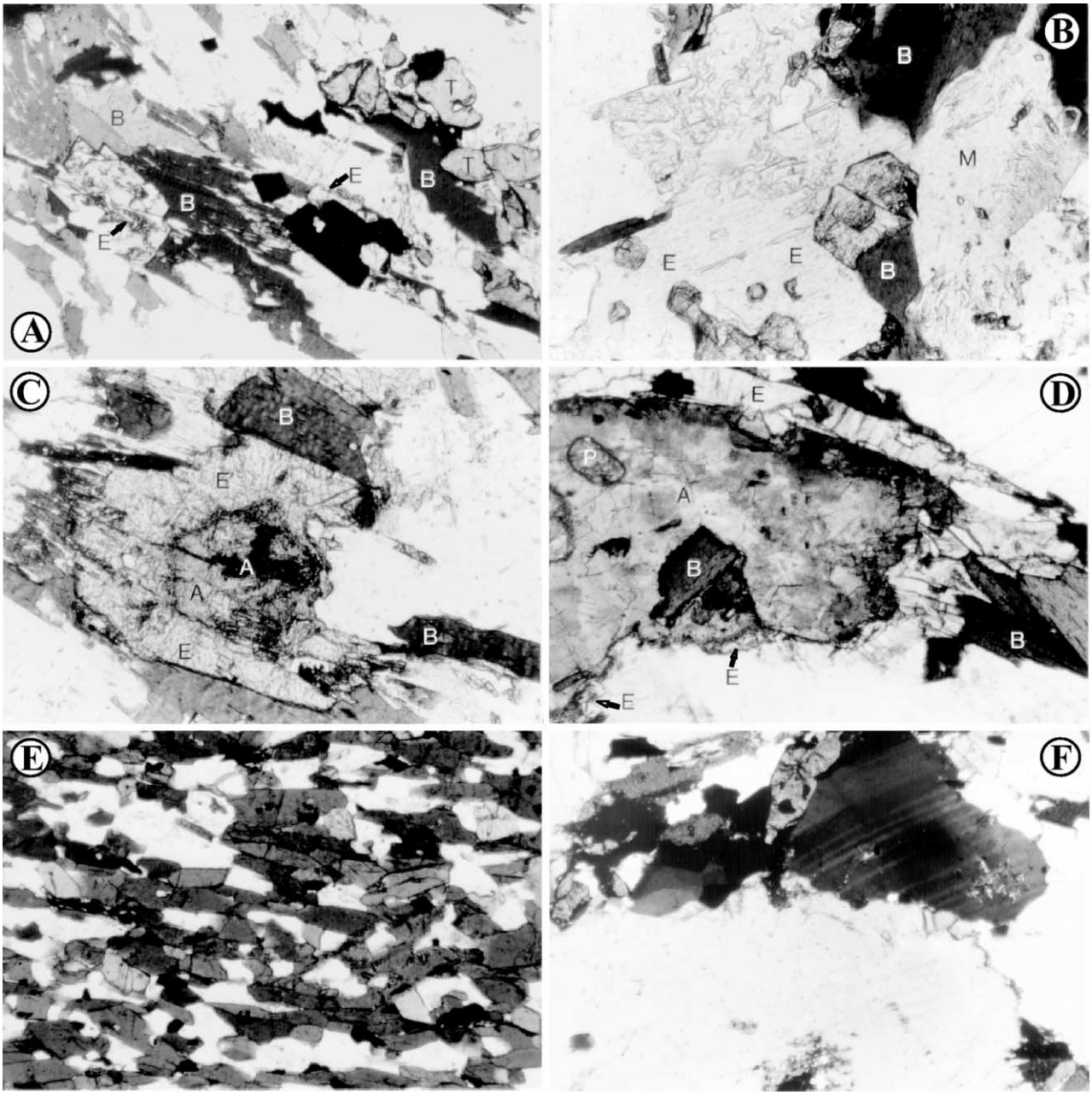

Figure 3. Photomicrographs; all but *D* from Douglas Harbour domain. *A*, Western Faribault-Thury complex tonalite 98-3070A, plane light. Epidote (*E*) is euhedral when armored by biotite (*B*) but corroded when exposed to the quartzofeldspathic matrix (*white*). *T* = titanite; black grains are Fe-Ti-oxides and small euhedral white grains are apatite. Field of view is 5 mm wide. *B*, Eastern Faribault-Thury complex potassic trondhjemite 98-2200A, plane light. Note the numerous euhedral allanite + epidote grains *E* hosted by muscovite (*M*), which shows corroded surfaces when exposed to the quartzofeldspathic matrix (*white*). *B* = biotite. Field is 1 mm wide. *C*, Trondhjemite 98-2200A, plane light. Note euhedral allanite (*A*) core to epidote (*E*) and corroded end of grain where unarmored by biotite (*B*). Allanite is less corroded than epidote, perhaps because of the low solubility of Th and REE in polymerized felsic melts. Field is 1 mm wide. *D*, Goudalie domain, Lac La Potherie tonalite 99-128, plane light. Large anhedral, metamict allanite core has a discontinuous epidote rim. However, each part of the rim has the same crystallographic orientation, indicating that they were once a single overgrowth. Note the euhedral biotite (*B*) and plagioclase (*P*) inclusions in the allanite. Field is 5 mm wide. *E*, Western Faribault-Thury complex, amphibolite-grade metabasalt 98-5059A. Plane light, field is 5 mm wide. Note alignment of hornblende grains (*dark prisms*), all with very similar crystallographic orientations as a result of recrystallization synchronous with deformation. *F*, Western Faribault-Thury complex tonalite 98-3070A. Note the serrated, high-energy, feldspar-feldspar grain boundaries. Crossed polars, field is 5 mm wide.

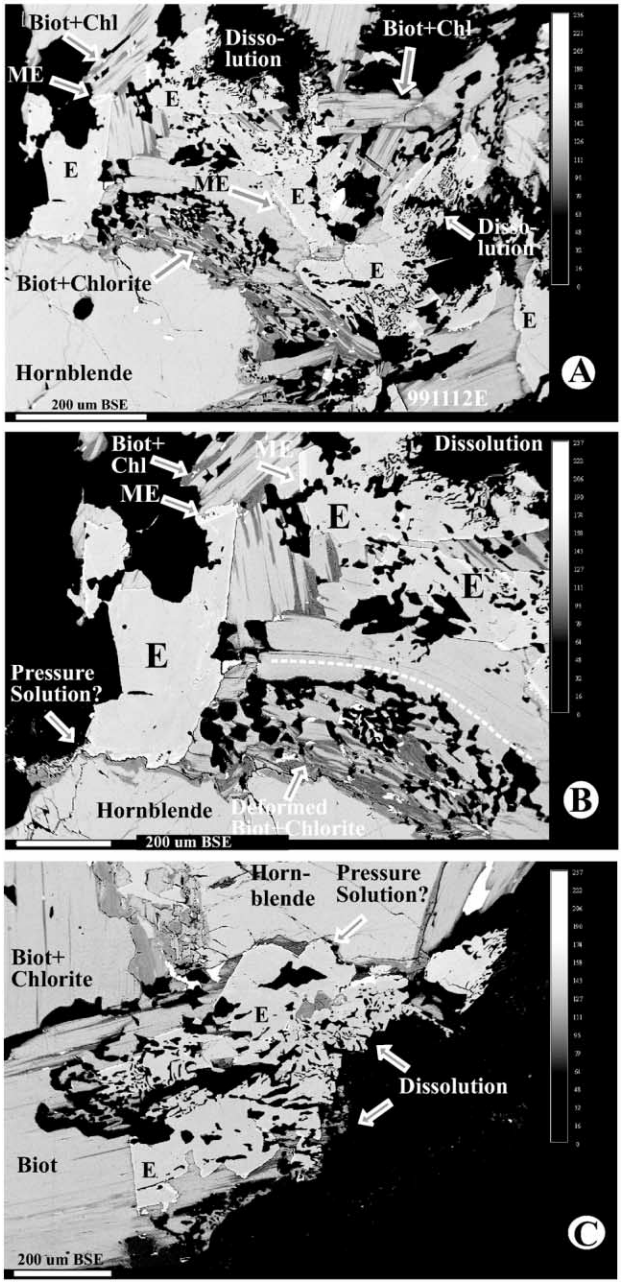

Figure 4. *A–C*, Clinopyroxene-tonalite 99-1112 (Lac Aigneau). *B*, Close-up of *A*. Epidote grains are faceted and euhedral when armored by biotite but display resorption structures when exposed to the quartzofeldspathic matrix. Note the high-reflectivity (Fe-rich) metamorphic epidote rim on the igneous epidote grains. The darker grey lamellae in biotite are chlorite. Note the deformation of biotite and chlorite, particularly to the right of the large epidote in *A* and *B*. Note the serrated contact between the epidote and hornblende and the rounded points on the epidote grains. These are interpreted to be due to pressure solution during deformation.

Proterozoic deformation and regional amphibolite-grade metamorphism has transformed some eastern Faribault-Thury complex TT series rocks into orthogneisses (Madore and Larbi 2000). In the process, epidote lost its igneous morphology and acquired a prismatic habit. The metamorphic epidote lacks allanite cores, may form rosettes, and does not show the characteristic resorption structures against quartz and feldspar. Deuteric/hydrothermal epidote is deep apple green in thin section, overgrows pale green igneous epidote, and is typically associated with chlorite (fig. 4).

Trondhjemite has <10% ferromagnesian minerals, principally biotite, with traces of the same accessory phases found in tonalite. In other respects, trondhjemite closely resembles tonalite. Several metapelite-dominated supercrustal belts are cut by trondhjemite pegmatites that contain tourmaline (black), garnet (pale pink), muscovite (pale green), and biotite.

Schlieren of diorite or hornblende gabbro (30%–50% ferromagnesian phases) within tonalite or trondhjemite are common. Rare intrusive bodies (~100–200 m) are massively to weakly foliated, heterogeneous in mode and grain size, and may contain angular clasts of tonalite and pyroxenite. Lath-shaped feldspar may show concentric zoning. Hornblende may be euhedral and contain clinopyroxene cores. Biotite typically rims hornblende. Accessory ilmenite, apatite, and titanite are commonly abundant (mineral lists in this article are given in order of abundance). Rare metamict allanite and interstitial quartz may be present, but there is no igneous epidote.

Granodiorite-Granite (GG) Series. Granite and granodiorite (GG) dominate the Utsalik, Lepelle, and Lac Minto domains. Most belong to the Leaf River Suite (Stern et al. 1994) and commonly occur as large homogeneous intrusions with igneous fabrics. Heterogeneous rocks containing abundant mafic pods and surmicaceous enclaves in various states of anatexis, disaggregation, and hybridization are common (Madore and Larbi 2000; Berclaz et al. 2001; Leclair et al. 2001; Simard et al. 2001). Interlayered granodiorite-granite commonly has fabrics and outcrop-scale structures very similar to the interlayered tonalite-trondhjemite described above (Madore et al. 2001). Granodioritic augen gneiss is common near major shear zones, and there are widely distributed, undeformed, granitic pegmatite dikes. Granodiorite generally has >10% alkali feldspar and contains hornblende + biotite, while granite has >20% alkali feldspar and contains only biotite. Granite and granodiorite locally contain alkali feldspar phenocrysts. Myrmekite is common.

Minor epidote, muscovite, Fe-Ti-oxides, titanite, allanite, and apatite are common, but garnet is rare. Textural relationships among trace phases are similar to the TT plutons.

The Enderbitic (E) Series. Enderbitic series plutons are widespread. They are dominantly mela-enderbite (orthopyroxene-tonalite) and leuco-enderbite (orthopyroxene-trondhjemite), typically with both clino- and orthopyroxene. Orthopyroxenite, gabbro-norite, pyroxene diorite, orthopyroxene-granodiorite (opdalite), and granite (charnockite) are subordinate. Massive, homogeneous enderbite intrusions show little modal or textural variation over many kilometers. More commonly, mela- and leuco-enderbite are interlayered on a centimeter-to-meter scale. Veins of unfoliated or weakly foliated leuco-enderbite may form reticulated networks that crosscut transpositional layering (fig. 6*A*), occupy strain shadows around xenoliths (fig. 6*B*), or are injected along shear zones (fig. 6*B*). As for the TT suite rocks, these features suggest synmagmatic deformation, with structural control on migration of leuco-enderbite melt. Enderbite typically shows a N-NNW-striking foliation with a steep dip and a subvertically plunging mineral lineation. It is common to find swarms of mela-enderbite or pyroxene diorite enclaves within leuco-enderbite. Amphibolite-grade metabasite xenoliths are cut by enderbite dikes, and orthopyroxene reaction rims are developed at the contacts (fig. 6*B*; cf. Percival et al. 1992).

Enderbites contain plagioclase + quartz + orthopyroxene + clinopyroxene ± hornblende + biotite + Fe-Ti-oxides + apatite + zircon. Textures of feldspars and quartz in enderbite closely resemble those in the TT series. Antiperthites are common (fig. 6*C*). In the least-deformed facies, quartz is interstitial (fig. 6*C*), and plagioclase is euhedral. With progressive deformation, quartz develops kink-bands, subgrains, and finally is reduced to a neoblastic mosaic, while plagioclase acquires high-energy, high-temperature, serrated grain boundaries. Orthopyroxene and clinopyroxene are commonly euhedral and prismatic, but clinopyroxene may be interstitial or absent. Bright red biotite and granular magnetite + ilmenite ± rutile are ubiquitous and abundant. Green hornblende rims clinopyroxene. Minor apatite and zircon are common, but accessory igneous titanite and epidote are absent.

The Clinopyroxene-Tonalite and Orthopyroxene-Tonalite (CT and OT) Series. Pyroxene-bearing hornblende-tonalite is common in the Utsalik and Lac Minto domains, typically associated with enderbite. Dioritic to gabbroic subfacies are subor-

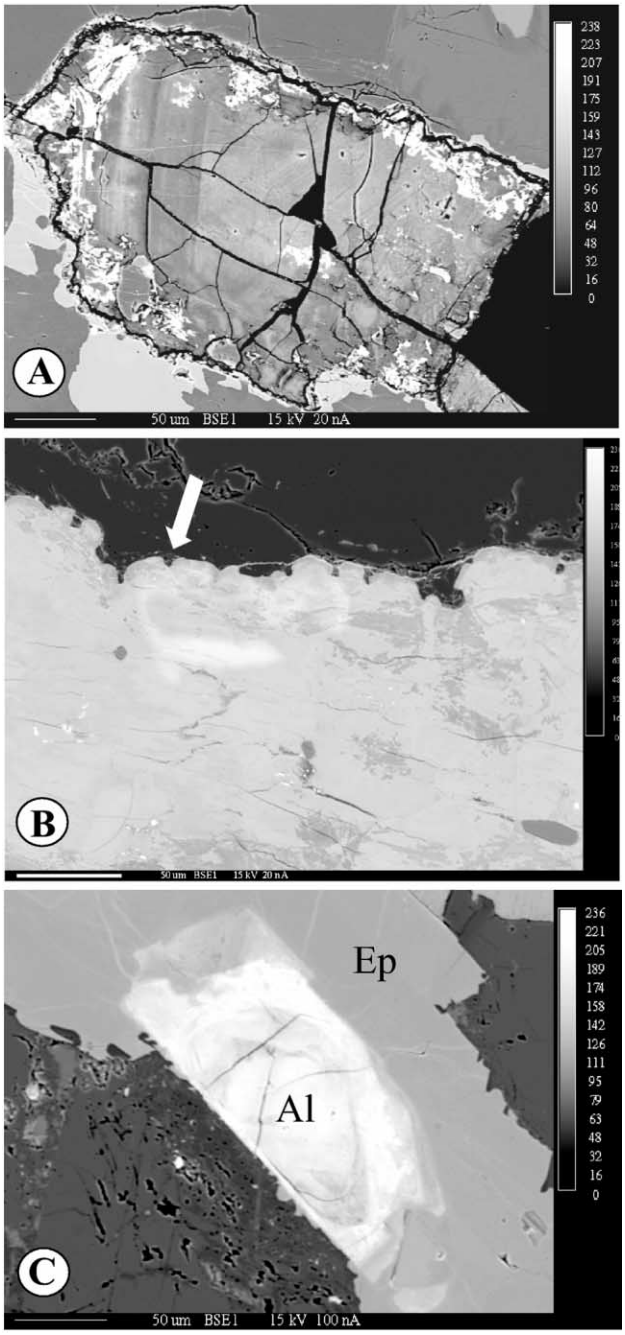

Figure 5. Electron backscatter images. *A*, Partially resorbed allanite from tonalite 99-218 (Lac La Potherie). Note the fine, concentric, lamellar igneous growth zoning and the irregular outline of the grain. The high-reflectivity borders are Th-rich phases that may be by-products of partial magmatic resorption. *B*, Edge of partially resorbed metamict allanite from tonalite 99-8509B (Lac Maricourt). The morphology of the grain edge resembles dissolution pits (*arrow*). *C*, Zoned allanite core in igneous epidote from tonalite 99-1246A (Lac La Potherie). Note concentric structure and high reflectivity zones (Th-REE-rich).

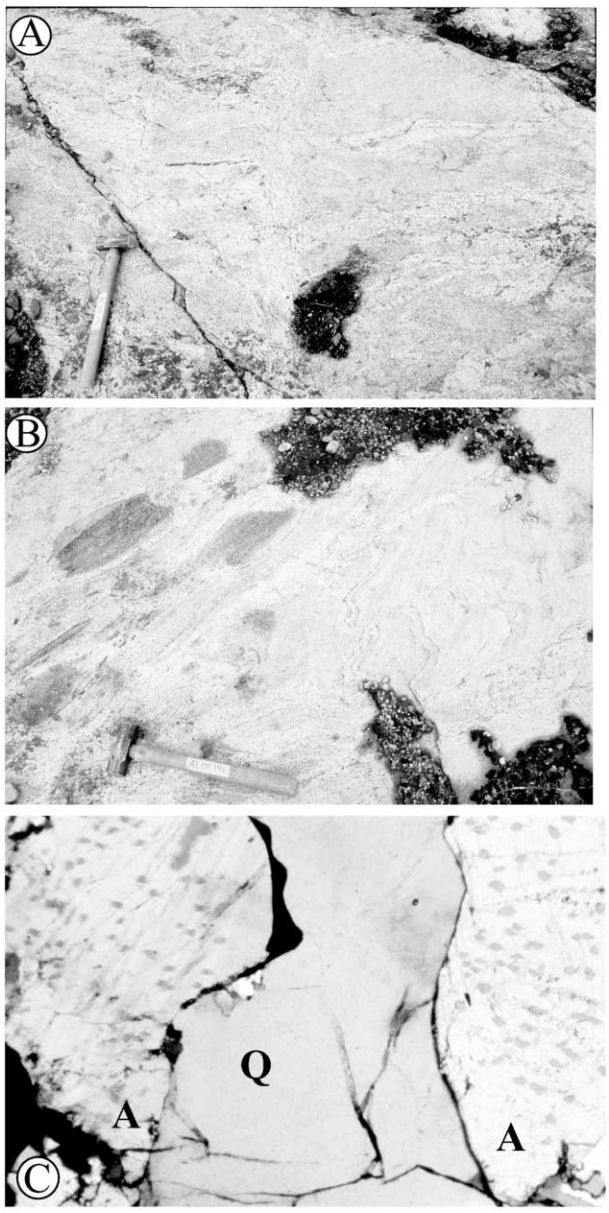

Figure 6. Field photographs and micrographs. *A*, Reticulated network of leuco-enderbite segregation veins in an enderbite from the Lac Vernon area. The vertical vein in the center of the picture is slightly sheared, suggesting a structural control on segregation. *B*, Amphibolite enclaves (upper left) with pyroxene-rich reaction rims in an enderbite from the Lac Vernon area. In center right, the mafic/felsic layering has been deformed. Oblique leuco-enderbite segregations cross the layered enderbite from the bottom left to the upper right, and probably were injected into a dilatant high-strain zone. Leuco-enderbite appears to fill strain-shadows around the mafic enclaves. *C*, Douglas Harbour domain, Troie complex enderbite 98-5042A. A pair of near-euhedral antiperthitic plagioclase grains are separated by interstitial quartz (*white*) and Fe-Ti oxide. Crossed polars, field of view is 5 mm wide.

dinate. The CT series rocks may form kilometer-scale aureoles around enderbitic cores (Gosselin and Simard 2001). Rocks of the CT and OT series are distinguished from the E series by having more abundant hornblende, a single pyroxene, and weaker biotite coloration. Field relationships and petrographic characteristics of CT and OT rocks are very similar to the TT series, save that pyroxene cores in hornblende are ubiquitous, while igneous epidote and muscovite are less common. In one, rock epidote and hornblende are in contact (see fig. 4). Rounding of epidote facets and deformation of intergranular mica + chlorite suggest that amphible and epidote were brought into contact by deformation, and that pressure-solution of epidote occurred.

Late Monzonite, Granite, Diorite and Gabbro-Norite in the Troie Complex (MZ Series). Most of the small mafic intrusions dispersed throughout the Troie complex in the Douglas Harbour domain (fig. 1) are pyroxene-diorite or gabbro-norite of shoshonitic affinity (Madore et al. 1999). Abundant (~10%–15%) Fe-Ti-oxides are diagnostic. Hornblende gabbro-norite is more strongly deformed than mica diorite. Mica diorite contains up to 20% of euhedral, zoned, antiperthitic plagioclase phenocrysts and 10% biotite phenocrysts, typically aligned parallel to intrusion contacts, indicating magmatic flow. Isolated gabbro-norite to diorite bodies may be massive, with the grain size coarsening inward, and internal segregation veins of leuco-norite to near-pure Fe-Ti-oxide. Agmatitic complexes are common, with gradations from sharply bounded mafic dikes with chilled margins, to swarms of centimeter- to meter-scale ovoid or lobate mafic enclaves embedded in enderbite, tonalite, or monzonite, which are interpreted to be disaggregated intraplutonic dikes (Hibbard and Watters 1985; Pitcher 1991). Rare potassic pyroxenite and harzburgite form discrete lenses (sheared dikes or metalavas?) in felsic hosts, or are associated with supercrustal belts.

Large, north-trending, steeply dipping intrusive sheets of late- to postkinematic porphyritic monzonite and quartz monzonite (5–10 km wide, up to 40 km long) constitute ~15% of the Troie complex. Associated minor monzo-diorite and abundant granite, with characteristic blue quartz, are generally massive and have sharp intrusive contacts against monzonite. Shoshonitic gabbro-norite to diorite plugs, dikes, and agmatite complexes are typically concentrated at the periphery of monzonite sheets and also cross-cut them. Monzonite and quartz monzonite intrusions contain 1–10-cm-sized euhedral phenocrysts of alkali feldspar, pla-

gioclase, and, locally, embayed quartz. Hornblende, biotite, and Fe-Ti-oxides are the dominant mafic minerals.

Supercrustal Belts. All Minto Block domains contain supercrustal belts. Most are small (<1 km wide), and a coherent internal stratigraphy is rarely preserved. Decameter- to kilometer-scale fold closures are apparent in several belts, typically with subvertical hinges and lineations. Fabric orientations in supercrustal and adjoining plutonic rocks are similar. Metabasalts and metapelites dominate, with locally abundant ironstone, metakomatiite, cumulate metapyroxenite and metaperidotite, metasandstone, metaconglomerate, felsic metatuffs, and marble. Pillow lavas, sedimentary bedding, and clasts in tuffs are locally preserved. Metabasalt typically shows evidence of incipient anatexis, with thin trondhjemitic veinlets lined by hornblendite. Where adjoining plutonic rocks belong to the TT or GG series, supercrustal rocks are dominantly of amphibolite grade. Where adjoining plutons are enderbitic, most supercrustal rocks have granulite-grade assemblages, and metasediments grade into garnetiferous and cordierite-bearing diatexite migmatites (Parent et al. 2002; cf. Kriegsman 2001). The largest belts may preserve coherent stratigraphic relationships (Percival et al. 1993; Skulski and Percival 1996) and show concentric zonation of apparent metamorphic grade, with greenschist-facies rocks in the center and higher grade rocks toward the contacts with intrusive plutonic rocks. Postpeak metamorphism faults and shear zones may juxtapose assemblages of different metamorphic grade (Percival and Skulski 2000; Percival et al. 2001). Mineral assemblages and textures in metasedimentary rocks are presented by Bégin and Pattison (1994) and Percival and Skulski (2000). Metapyroxenites and metaperidotites are described in Madore et al. (1999).

The dominant texture in amphibolite-grade metabasalt ranges from granoblastic polygonal to nematoblastic, to protoclastic. Commonly, elongate hornblende grains in a thin section share the same pleochroism and extinction angle (fig. 3*E*), implying extensive syndeformation recrystallization (Cumbest et al. 1989; Kruse and Stünitz 1999). In granulitic metabasalt, most pyroxene and feldspar have straight or gently curved grain boundaries and 120° triple junctions, indicating complete recrystallization and reequilibration. Most commonly, green hornblende in granulitic metabasalt forms a mosaic with plagioclase and pyroxene, with rare rims on pyroxene that suggest it is replacive. Hornblende may also be concentrated into centimetric lamellae or veins that alternate with granulitic assemblages. Retrogression caused by channelized penetration of water seems likely. Other metabasaltic rocks, however, preserve evidence of prograde amphibolite to granulite reactions.

Mineral Chemistry

Only data pertinent to thermobarometric calculations, or to the attribution of an igneous versus metamorphic origin to a mineral species are presented. Data specific to the Douglas Harbour domain is presented in Bédard et al. (2003).

Pyroxenes. Clinopyroxene generally has Mg# (100 Mg/Mg + Fe^{2+}) between 62–78 (table A1), with shoshonitic mica diorites ranging to Mg# (59). All clinopyroxene has TiO_2 between 0.05 and 0.28 wt%; Al_2O_3 between 0.95 to 2.6 wt%; and low Fe^{3+}/Fet and Al^{vi} calculated assuming stoichiometry. Most orthopyroxene has Mg# between 45 and 65; Al_2O_3 between 0.5 and 1.7 wt%; TiO_2 between 0.02 and 0.15 wt%; with low Fe^{3+}/Fet, Al^{vi}, and Wo. Harzburgite 98-1062C (Douglas Harbour domain) has high-Al_2O_3 (1.6%–2 wt%) enstatite (Mg# 89-91).

Amphibole. Tonalite and trondhjemite contain magnesian hastingsitic or tschermackitic hornblende (nomenclature after Tindle and Webb 1994) with TiO_2 between 0.5 and 1.8 wt% and Al_2O_3 between 8 and 12 wt% (table A2). Hornblende in shoshonitic diorite extends to lower TiO_2 (0.3 wt%) and Al_2O_3 (7 wt%), with these elements increasing as MgO decreases. Shoshonitic gabbro-norite and diorite generally contain magnesian hastingsitic hornblende (TiO_2 = 1–2.3 wt%; Al_2O_3 = 8.7–11.4 wt%). Amphibole in a Troie complex quartz monzonite straddles the magnesian hastingsitic/ferroedenitic divide and has low Al_2O_3 (9.2–9.6 wt%). Enderbite has magnesian hastingsitic to edenitic hornblende, with TiO_2 (2.1–2.4 wt%) higher than in typical tonalite, though Al_2O_3 is similar (9–11 wt%). Amphibole in CT tonalite is similar to TT series amphibole in terms of TiO_2 (0.6–1.8 wt%) and Al_2O_3 (8–12 wt%) but tends to be more magnesian. Amphibole Na_2O and K_2O contents generally increase as MgO decreases. Shoshonitic pyroxene diorite and gabbro-norite has higher-K_2O (1.4–1.85 wt%) amphibole. Tremolitic hornblende in metakomatiite has low Al_2O_3 (4.7–5.8 wt%), Na_2O, and K_2O.

Feldspars. Plagioclase shows limited Or- (<2 mol%) and SrO (<0.3 wt%) ranges (table A3), with SrO decreasing with An. Plagioclase in tonalite and trondhjemite (TT series) has a limited An range (An_{36-16}), and weak normal or reversed zoning is common. Rare euhedral phenocrysts are normally

zoned (e.g., $An_{38.5-32}$). More sodic compositions (to An_2) are inclusions in epidote (subsolidus Ca-loss?), exsolution blebs in orthoclase, or deuteric (?) groundmass material. Plagioclase in associated TT-series diorite ranges to An_{54}. Plagioclase in granodiorite (An_{28-18}) and granite (An_{22-12}) show a range similar to tonalite and trondhjemite, respectively. Enderbitic rocks have plagioclase between An_{34-26}, with plagioclase in associated gabbro-norite ranging to An_{54}. Plagioclase in pyroxene-bearing (CT-OT) tonalite and diorite shows a similar range (An_{44-22}). Shoshonitic hornblende gabbro-norite and mica diorite have An_{56-26} and An_{32-24} plagioclase, respectively. A Troie complex quartz monzonite contains euhedral An_{25} plagioclase.

Most alkali feldspar is orthoclase-rich (Or_{93-98}, $An_{<0.05}$, $Cs_{1.5-2}$), reflecting near-complete low-temperature exsolution (table A3; fig. 7). Weak zoning may be normal or reversed (1%–2% An). Evolved granite has essentially Ba-free orthoclase. A Troie complex quartz monzonite has fine exsolved microperthite. When analyzed in raster mode, these show a wider compositional spectrum (Or_{64-81}, $An_{0.2-2.2}$, $Cs_{1.2-2.4}$). Raster analyses of fine perthite in enderbite by Percival and Mortensen (2002) yielded An-contents as high as 8.6.

Muscovite. Muscovite typically has high FeO^* (4.5–6 wt%) and TiO_2 (0.5–1.7 wt%; table 1; fig. 8). Celadonite solid solution is extensive, with limited replacement by the sodic end-member. Compositions are appropriate for igneous muscovite (>0.6 wt% TiO_2; Miller et al. 1981; Speer 1984; Zen 1988). Garnet-two-mica granite (98-3102A) and trondhjemitic garnet-tourmaline-two mica pegmatite (98-3134D) from the Faribault-Thury complex have muscovite with lower FeO^* (<4.5%) and TiO_2 (<0.5%), a pattern that probably reflects increases in melt aluminosity (Zen 1986; Hogan

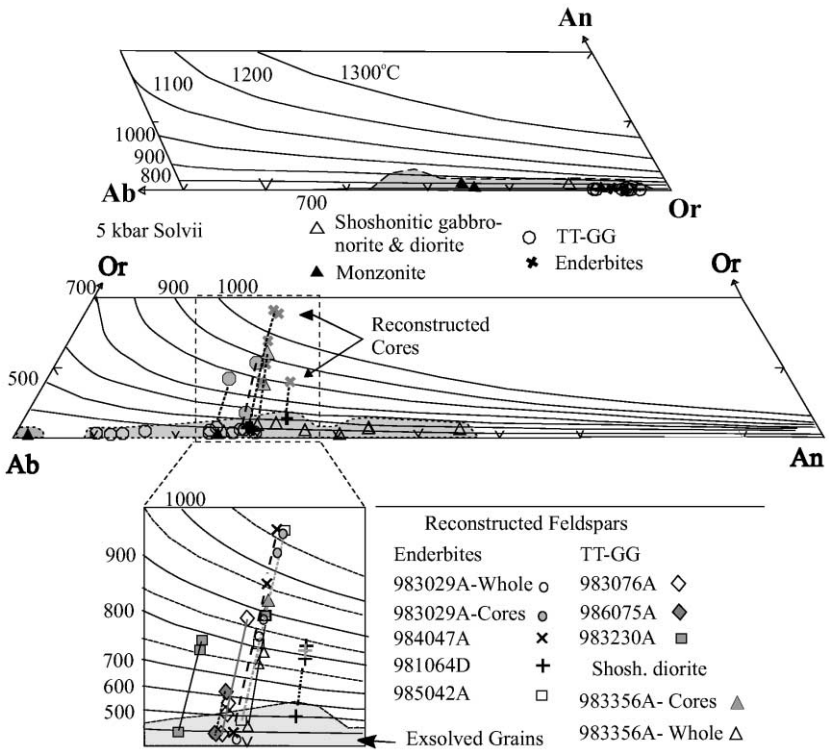

Figure 7. Feldspar compositions from Douglas Harbour domain (Lac Peters) rocks plotted in the albite-anorthite-orthoclase system. Data from other domains show similar distributions. Isotherms calculated from Wen and Nekvasil (1994) at 5 kbar. In the top and middle diagrams, points show average analyses for gabbro-norites (Troie complex), monzonite series rocks (Troie complex), TTG (tonalites and trondhjemites), and enderbites (Troie complex and Qimussinguat complex). Shaded fields represent all data. Gray symbols in the middle diagram show compositions of reintegrated analyses (see fig. 10 and text for method), linked to exsolved plagioclase compositions by dotted tielines. *Bottom*, reintegrated data in more detail, with each point representing an individual reintegrated grain, or grain core. Tielines join these reintegrated data to analyzed feldspar (lowermost point of each type). Note the clustering of individual points from each rock.

Table 1. Representative Average Muscovite Compositions

	Douglas Harbour domain				Lac La Potherie		Lac Vernon
	Garnet granite 98 3102A	Granodiorite 98 2200A	Granodiorite 98 3300A	Garnet trondhjemite 98 3134D	Trondhjemite 99 1250C	Granodiorite 99 5122A	Trondhjemite 00 2202A
N	5	7	5	8	12	6	1
SiO_2	46.49	45.96	46.43	45.92	46.27	46.61	46.17
Al_2O_3	32.11	29.72	30.20	36.00	29.43	30.15	30.56
TiO_2	.23	1.09	1.02	-dl	.79	1.15	1.17
FeO^*	3.73	5.63	4.89	1.97	5.70	5.15	5.16
MnO	.06	.04	.05	-dl	.04	.03	.02
MgO	1.43	1.48	2.10	.32	1.95	1.52	1.46
CaO	-dl	-dl	.03	-dl	.03	.02	.03
Na_2O	.19	.19	.19	.33	.17	.17	.25
K_2O	10.31	10.27	10.08	10.40	9.92	10.02	10.81
BaO	-dl	-dl	-dl	-dl	-dl	-dl	.17
H_2O	4.37	4.31	4.36	4.47	4.33	4.35	4.41
Total	97.84	98.88	99.48	99.53	98.75	99.35	100.27
Si	7.198	7.191	7.190	7.038	7.239	7.258	7.103
Alt	5.861	5.483	5.513	6.506	5.428	5.535	5.542
Al^{iv}	.802	.809	.810	.962	.761	.742	.897
Al^{vi}	5.058	4.674	4.704	5.545	4.666	4.793	4.645
Fe	.483	.737	.634	.252	.746	.670	.663
Ti	.027	.128	.119	…	.092	.135	.135
Mg	.329	.346	.484	.072	.454	.353	.334
Mn	.007	.005	.007	…	.006	.004	.002
Ca	…	…	.005	…	.005	.003	.005
Na	.058	.059	.058	.097	.051	.051	.075
K	2.036	2.050	1.991	2.034	1.980	1.991	2.121
Ba	…	…	…	…	…	…	.011

Note. All iron assumed to be FeO. Water calculated from the Cameca SX100 software. Structures calculated assuming 24 anions.

1996) and depletion of the melt in FeO^* and TiO_2 during fractional crystallization.

Allanite and Titanite. Allanite is commonly metamict but still yields reasonable analyses (tables 2, A5; fig. 9), with generally high rare-earth and thorium contents. Some grains show systematic concentric decreases in rare-earths and thorium, marking a gradation toward surrounding epidote overgrowths, a pattern compatible with fractional crystallization processes (Bédard et al. 2001). Titanite contains elevated rare-earth contents (table 2).

Epidote grains that I interpret as magmatic show a restricted compositional range (pistachite 25-30; tables 2, A5; fig. 9) typical of igneous epidote (Zen and Hammarstrom 1984; Evans and Vance 1987; Dawes and Evans 1991). In contrast, apple- to bottle-green metamorphic/deuteric epidote rims generally have higher Ps-contents (table 2; fig. 9), especially when associated with chlorite after biotite (cf. Dahlquist 2001). Some tonalitic orthogneisses from the eastern Faribault-Thury complex that were affected by Proterozoic deformation and amphibolite-grade regional metamorphism contain prismatic metamorphic epidote with Ps-contents (25–30) similar to those of igneous-textured epidote.

Geobarometric and Thermometric Constraints

For Al-in-hornblende geobarometry, pressures were calculated using various formulations of the Al-in-hornblende geobarometer for rocks containing the requisite buffering assemblage (hornblende + biotite + titanite + magnetite + plagioclase + alkali feldspar + quartz). The Johnson and Rutherford (1989) and Hammarstrom and Zen (1986) calibrations yield similar results (table 3). Relative to the Hammarstrom and Zen (1986) formulation, the Anderson and Smith (1995) calibration gave values up to 2 kbar lower, while the Schmidt (1992) calibration gave values up to 1 kbar higher. The Schmidt (1992) formulation was used to facilitate comparison with the results of Percival and Skulski (2000) and Percival et al. (1992).

Most calculations for TT, GG, OT, and CT series rocks yield pressures between 4 and 6.4 kbar (table 3), in agreement with previous estimates from elsewhere in the Minto Block using the same barometer and calibration (3.5–5.6 kbar: Percival et al.

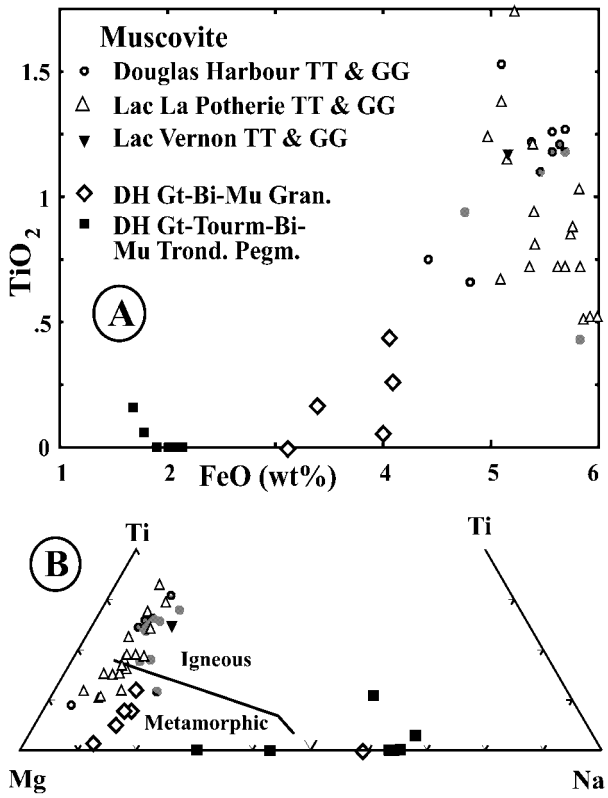

Figure 8. Muscovite analyses. *DH* = Douglas Harbour. Note that only muscovites from the extremely evolved garnet granite and trondhjemites are depleted in TiO_2 and FeO^*, presumably due to prior fractionation of magnetite and ilmenite. The division into the metamorphic/igneous field is from Miller et al. (1981).

1992; 3.8–6.5 kbar: Percival and Mortensen 2002) and with estimates based on metamorphic mineral assemblages in supercrustal belts (typically 2–5 kbar but locally up to 8–10 kbar: Percival and Berman 1996; Percival and Skulski 2000; Baille-Barrelle et al. 2000; Madore et al. 2001). The TT series rocks from the Faribault-Thury complex yield higher (~1 kbar) pressures than plutonic rocks from elsewhere in the Minto Block, suggesting deeper exhumation. However, monzonite, and shoshonitic diorite (~2.72–2.7 Ga) from within the Troie complex yield pressures similar to other Minto Block domains (5–6.2 kbar). The 1-kbar difference between older Faribault-Thury rocks and adjoining younger Troie rocks suggests about 3 km of decompression between 2.88 and 2.7 Ga and implies a very modest exhumation rate of about 0.2 mm/yr, when compared to exhumation rates characterizing active Phanerozoic orogens (1–34 mm/yr; Burbank 2002).

For pyroxene geothermometry, the QUILF geothermometer (Andersen et al. 1993) gave fairly uniform two-pyroxene temperatures (713°–864°C at 5 kbar assumed pressure; table 4), with more dispersion for single pyroxene determinations (697°–911°C). These values are in general accord with hornblende-plagioclase temperatures and imply near- or suprasolidus conditions for TT and GG suite rocks. An ultramafic cumulate from the Douglas Harbour domain gave 801°C using the CaO-in-orthopyroxene thermometer of Brey and Köhler (1990) at 5 kbar assumed pressure.

The Blundy and Holland (1990) plagioclase-hornblende thermometer gave temperatures between 666° and 793°C for TT and GG series rocks, and 744°C for a Troie monzonite (table 3; 5 kbar assumed). Rocks of the CT-OT series yield a similar range (723°–783°C). Hornblende-bearing enderbite (801°–948°C) and shoshonitic gabbro-norite and diorite (760°–826°C) record higher temperatures. For magnetite-ilmenite thermometry, calculations using the QUILF geothermometer/oxygen barometer yield low, subsolidus temperatures (generally <400°C) for oxide pairs in all rocks.

Most Minto Block feldspar falls along low-temperature (<500°C) solvii (fig. 7; table 4), indicating extensive subsolidus reequilibration. Image-analysis reconstruction of preexsolution antiperthite grains (figs. 7, 10; table 4) were used to estimate initial crystallization temperatures (Raase 1998). Multiple grains in individual rocks generally gave similar results, indicating that the procedure is reproducible. Larger grain-to-grain variations reflect either a range of initial feldspar compositions, variable subsolidus reequilibration, or simply a misfit between the thin section plane and zoned grains. Comparison with 5 kbar solvus compositions calculated using SOVCALC2 (Wen and Nekvasil 1994) indicate plagioclase crystallization temperatures of 550°–870°C in TT and GG series rocks, 810°–1045°C in enderbite, and 910°C (cores) and 760°C (bulk phenocrysts) in a shoshonitic mica diorite. The high enderbite temperatures (>810°C, 4 rocks) are noteworthy, since antiperthite grains in most TT/GG series rocks yield temperatures <800°C, with a single determination at ~870°C. The fragility of these antiperthite exsolution textures suggest largely static cooling between the temperature indicated by reconstruction, and the final solvus temperatures attained (Frost et al. 1989).

Discussion

Metamorphic or Magmatic Origin of Minerals and Fabrics in Felsic Plutonic Rocks. Existing models

Table 2. Representative average epidote, allanite, and titanite compositions

	Lac Aigneau, tonalite (99-1110A2)		Lac Maricourt, trondhjemite (99-8509A)			Lac La Potherie							
						Trondhjemite (99-215)		Trondhjemite (99-1246A)		Granodiorite (99-218)			
	I	A	M	I	A	M	I	I	A	I	A	T	T
N	16	2	1	2	4	6	8	6	7	4	5	17	38
SiO_2	37.73	36.25	37.55	37.91	30.82	37.18	37.89	37.24	30.54	36.81	33.39	29.74	3002
Al_2O_3	23.02	16.70	20.37	23.13	15.60	19.13	23.38	22.81	14.25	22.52	19.91	1.21	1.35
TiO_2	.09	.01	.17	.11	.72	.12	.09	.11	.62	.05	1.43	35.96	36.22
FeO	.43	…	.91	1.17	10.73	.53	.37	1.28	10.42	…	14.80	1.79	1.64
Fe_2O_3	13.66	16.15	17.20	13.14	2.01	18.83	13.54	12.13	3.94	15.53	2.05	…	…
$Fe_2O_3^*$	14.14	16.15	18.22	14.44	13.94	19.42	13.96	13.56	15.53	15.53	18.52	…	…
MnO	.18	.08	.23	.23	.48	.08	.36	.19	.32	.21	.13	nd	nd
MgO	.01	11.18	.03	-dl	.89	.03	-dl	.04	.38	-dl	.62	nd	nd
CaO	23.07	12.04	22.42	22.61	9.23	22.70	22.98	22.04	10.09	23.02	4.01	26.51	27.11
Na_2O	nd	nd	nd	nd	nd	nd	nd	nd	nd	nd	nd	.02	.03
K_2O	.01	.07	.01	.01	.07	.01	-dl	.02	.09	-dl	.42	-dl	-dl
ThO_2	.009	-dl	.025	.019	1.74	.026	.022	.036	1.80	.024	2.68	-dl	-dl
La_2O_3	.015	.270	.012	-dl	7.05	.013	-dl	.194	4.95	-dl	.289	.168	116
Ce_2O_3	.037	.526	-dl	-dl	12.63	.025	-dl	.352	11.60	.014	1.63	.879	.787
Nd_2O_3	.057	.288	.112	.044	4.55	.070	.013	.261	4.40	.022	.185	.547	.527
ZrO_2	.006	.004	-dl	-dl	.078	-dl	-dl	-dl	.288	-dl	.044	-dl	-dl
P_2O_5	.005	.025	.006	.005	.007	-dl	-dl	-dl	.081	.003	.044	nd	nd
SrO	.043	-dl	.257	-dl	.398	.121	-dl	.137	.508	.195	-dl	nd	nd
Total	98.30	93.05	101.10	100.17	91.74	98.68	98.64	96.52	94.16	98.34	79.68	96.82	97.79
Si	3.003	2.958	3.007	3.016	3.130	3.007	3.002	3.025	3.061	2.943	3.395	…	…
Al	2.160	1.607	1.923	2.169	1.866	1.824	2.184	2.183	1.689	2.122	2.398	…	…
Fe^{3+}(t)	.847	.992	1.098	.865	1.064	1.182	.832	.828	1.173	.934	1.409	…	…
Fe^{2+}	.029	.000	.061	.078	.916	.036	.032	.090	.948	…	1.245	…	…
Fe^{3+}	.818	.992	1.037	.787	.148	1.146	.801	.739	.299	.934	.164	…	…
Ti	.005	.001	.010	.006	.056	.007	.005	.007	.047	.003	.107	…	…
Mg	.001	1.358	.003	…	.132	.004	…	.005	.057	…	.091	…	…
Mn	.012	.006	.015	.015	.041	.005	.024	.013	.027	.015	.011	…	…
Ca	1.967	1.054	1.924	1.927	1.003	1.967	1.951	1.916	1.083	1.972	.453	…	…
K	.001	.007	.001	.001	.009	.001	…	.002	.012	…	.053	…	…
Th	.0002	…	.0005	.0002	.039	.0002	.0001	.0007	.040	.0003	.035	…	…
La	.0004	.004	.0003	…	.255	.0001	…	.006	.183	…	.006	…	…
Ce	.001	.008	…	…	.453	.0002	…	.011	.426	.0003	.034	…	…
Nd	.002	.004	.0032	.0006	.159	.0007	.0001	.008	.158	.0005	.004	…	…
Zr	.0002	.0001	…	…	.004	…	…	…	.009	…	…	…	…
P	.0003	.001	.0004	.0002	.0006	…	…	…	.006	…	.002	…	…
Sr	.002	…	.012	…	.023	.0028	…	.007	.030	.007	…	…	…
Ps	.275	.381	.350	.266	.071	.386	.268	.253	.150	.306	.070	…	…

Note. Epidote and allanite structures calculated assuming eight cations and 25 oxygens. Pistachite component (Ps) = Fe^{3+}/Fe^{3+} + Al. Water calculated from the Cameca SX100 software. I = igneous epidote, M = metamorphic epidote, A = allanite, T = titanite.

(Lin et al. 1996; Percival and Skulski 2000; Percival et al. 2001) attribute deformation and metamorphism of Minto Block supercrustal belts to regional-scale collisional orogenesis, with complete recrystallization and transposition of fabrics into the dominant NNW regional grain. Tectonism on this scale must also have overprinted the plutons in which the supercrustal rocks are embedded and which share the same fabrics. Indeed, plutonic rocks in the Minto Block have historically been described as high-grade orthogneisses affected by regional metamorphism. The swarms of enderbitic intrusions are commonly interpreted as "high-grade granulite" terrains (Stevenson 1968; Card and Ciesielski 1986). Since orthopyroxene is commonly inferred to have formed during granulite-grade metamorphism, criteria must be found to decide whether E/OT series plutons in the Minto Block record granulite-grade metamorphism, or represent unusually dry, hot magmas (Kilpatrick and Ellis 1992; Frost et al. 2000).

Many Minto Block plutonic rocks preserve outcrop-scale structures that indicate synmagmatic deformation. For example, trondhjemite or leucoenderbite fill strain shadows and centimeter- to meter-scale shear zones within tonalite or melaenderbite, respectively (fig. 2*A*; fig. 6*A*, 6*B*). Similar features occur in rocks of the GG, CT, and OT series, indicating that evolved residual melts typically migrated along structurally controlled channels (cf. Vigneresse et al. 1996; Sawyer 2000). Additional support for synmagmatic deformation

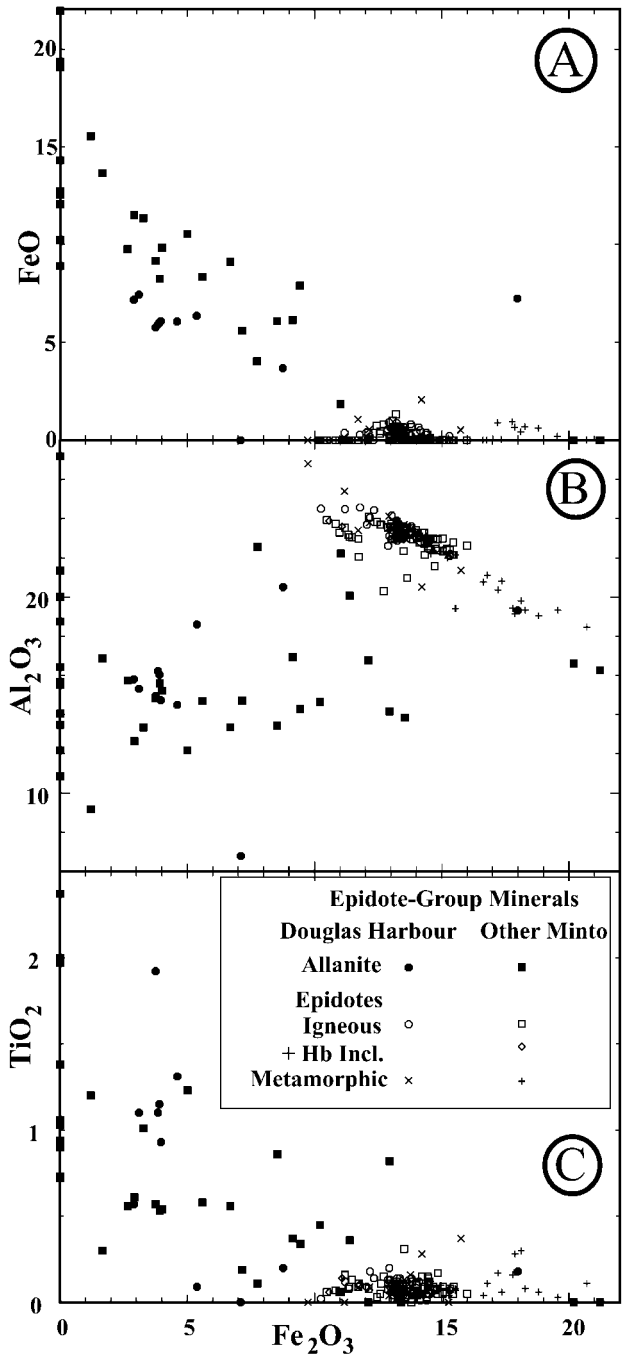

Figure 9. Epidote-group minerals. Open diamonds show composition of rare epidote grains from the Lac Vernon area that contain small hornblende inclusions.

is provided by variably deformed tonalitic enclaves in trondhjemitic breccia complexes and mingled melatonalite/trondhjemite intraplutonic dikes (fig. 2*C*) that show smaller degrees of deformation coaxial with that observed in the hosts. The fact that fabrics are rather homogeneous and penetrative (fig. 2*B*; Gapais 1989) also suggests a ductile (mushy) medium. Many enderbitic plutons have coarse, massive, homogeneous textures, locally with aligned phenocrysts, indicating magmatic flow (Percival et al. 1997; Percival and Skulski 2000). In addition, leuco-enderbite/charnockite dikes cut amphibolite (fig. 6*B*), which is inconsistent with a granulite-grade metamorphic origin for the enderbite (this work; Percival et al. 1992, 1993).

On the thin section scale, many features imply the preservation of a magmatic history, including (1) local preservation of lath shapes in plagioclase from TT-series diorite, with twins parallel to elongation (Vernon 2000); (2) an interstitial morphology for quartz in low-strain zones (fig. 6*C*); (3) the absence of coronitic structures (cf. fig. 3 with illustrations in St.-Onge and Ijewliw [1996]); (4) the lack of a crystallographic preferred orientation (fig. 3*A*) for mafic minerals in plutons, unlike the clearly metamorphic textures of metabasaltic amphibolite in supercrustal belts (fig. 3*E*); (5) early high-temperature euhedral clinopyroxene + orthopyroxene + biotite in E-series rocks, with late appearance of hornblende, a sequence of crystallization indicating cooling and progressive increase in a_{H_2O} during fractionation (Percival and Mortensen 2002); and (6) the interstitial habit of hornblende in E-series plutons, obviously inconsistent with a prograde metamorphic origin for pyroxene through amphibole breakdown.

In addition, pyroxene, plagioclase-hornblende, and reconstituted plagioclase geothermometers yield granulite-grade (700°–860°C) temperatures for hornblende- or epidote-bearing rocks, and near-liquidus temperatures for E-series plutons (810°–1045°C; table 4; fig. 7). In the context of a prograde tectonometamorphic event characterized by penetrative deformation/recrystallization, such high temperatures are probably inconsistent with the preservation of hornblende, and at these low pressures, perhaps also of epidote in TT series rocks (Thompson and Ellis 1994). Combining thermometric results with pressures derived from the hornblende barometer yields the *PT* conditions at which feldspar and hornblende in these rocks last equilibrated (fig. 11). Most determinations straddle the granitic to tonalitic solidus, in accord with an igneous origin.

Garnet (J. H. Bédard, unpublished values) and muscovite (table 1; fig. 8) both have "igneous" compositions, and titanite contains elevated rare-earth contents (table 2), typical for igneous titanite (Piccoli et al. 2000). Epidote has igneous compositions (Pistachite 25–30; table 2; fig. 9), may exhibit concentric growth zoning, and commonly has allan-

Table 3. Hornblende/Plagioclase Thermobarometry

	Al-Hbl barometer (kbar)				Hbl/Plag thermometer (°C)		
	HZ86	JR89	S92	AS95(3)	BH5kb	P = S92	P = AS95(3)
Douglas Harbour:							
Ultramafic lava:							
98-6193C	.4	.1	1.1	…	500	…	…
Hornblende gabbro-norites:							
982001D	5.1	5.4	5.6	3.5	779	780	788
983002A	5.4	5.7	5.8	2.9	805	807	818
983046B	5.9	6.2	6.3	2.7	826	828	835
983055B	5.0	5.2	5.4	2.7	796	798	814
Mica diorites:							
983013B	4.8	5.1	5.3	3.2	773	773	789
983356A	4.7	4.9	5.2	3.4	760	761	779
Quartz monzonite:							
983155A	4.6	4.8	5.0	3.7	744	744	760
TTG suite (hornblende diorite):							
997165D	6.0	6.4	6.4	5.4	735	735	735
TTG suite:							
983070A	5.3	5.6	5.7	5.2	711	712	711
983076A	6.1	6.4	6.4	5.3	745	748	745
986075A	5.6	5.9	6.0	5.4	715	714	714
993154A	6.0	6.3	6.3	5.1	750	751	750
Enderbite suite:							
981064D	5.0	5.2	5.4	…	948	951	…
Pelican-Nantais tonalite:							
008070AHb.Inc.	4.9	5.1	5.3	3.3	774	774	789 Plag.Core
008070AHbPhen.	5.1	5.3	5.5	3.3	777	775	794 Plag.Phen.
Lac Maricourt:							
Cpx-tonalite suite (pyroxene diorite):							
991190A	3.9	4.0	4.4	2.4	776	779	793
TTG suite (hornblende diorite):							
998518D	5.1	5.3	5.5	3.4	772	773	789
TTG:							
998504D	1.9	1.7	2.5	2.4	666	673	680
998506A2R	5.7	6.1	6.1	4.2	764	768	781
Lac Aigneau:							
Cpx-tonalite suite (pyroxene diorites)							
991103	4.0	4.1	4.5	3.7	723	724	733
991213A	5.4	5.7	5.8	3.4	783	785	798
TTG suite:							
991112A	3.6	3.6	4.1	2.5	754	758	777
991118B	4.8	5.0	5.3	3.5	762	763	778
Enderbite suite:							
991212A	6.0	6.3	6.4	3.9	801	800	799
994052A	4.9	5.1	5.3	2.5	796	797	816
Lac La Potherie:							
TTG suite:							
99213	4.4	4.6	4.9	4.2	718	717	727
Cpx-tonalite suite:							
991252A	4.2	4.4	4.7	3.6	734	735	751
Lac Vernon:							
TTG suite:							
002205A	5.4	5.6	5.8	4.4	744	742	755
TTG suite hornblende diorite:							
002208A	4.4	4.6	4.9	3.0	763	763	784
002209AHb.Inc.	3.8	3.8	4.2	2.8	762	763	770 Plag.Core
002209AHb.Phen.	1.8	1.6	2.4	2.2	681	686	691 Plag.Phen.

Note. Results of alternative formulations of the Al-in-hornblende thermometer from HZ86 = Hammarstrom and Zen (1986), JR89 = Johnson and Rutherford (1989), and S92 = Schmidt (1992). Temperatures for the AS95 barometer were taken from the Blundy and Holland (1990) thermometer, with three iterations. Results of hornblende/plagioclase thermometer of Blundy and Holland (1990) are for a 5 kbar pressure (BH5kb), or are set at the value given by the Al-in-hornblende barometer of Schmidt (1992; S92) or Anderson and Smith (1995; AS95) after three iterations.

Table 4. Pyroxene and Feldspar Thermometry (°C), 5 kbar assumed

	QUILF Fe/Mg/Ca in pyroxene(s)			SOVCALC2		
	2-Pyroxene	Cpx	Opx	Plag/AF	P	Reconstructed antiperthites
Douglas Harbour hornblende gabbro-norites:						
982001D	713 ± 52	900	697	…	…	…
983002A	773 ± 24	879	760	…	…	…
983046B	745 ± 29	845	733	…	…	…
983242B	…	806	…	…	…	…
983055B	…	773	…	…	…	…
Mica diorites:						
981058F	715 ± 7	730	714	…	…	…
983013B	732 ± 13	776	727	…	…	…
983356A	745 ± 11	776	742	556	5	910, average 2 cores 760, average 2 whole grains
Enderbite suite:						
981064D	733 ± 19	785	728	501	5	810, average 3 grains
983029A	797 ± 34	817	805	518	5	1045, average 2 cores 855, average 2 whole grains
984047A	826 ± 26	777	847	520	5	1010, grain 1 955, grain 2
985042A	…	755	…	…	5	1020, grain 1 890, grain 2 810, grain 3
TTG suite:						
983076A	…	…	…	535	5	870, 1 core 550, average 2 whole grains
983230A	…	…	…	525	3	760, average 2 grains
986075A	…	…	…	630	5	…
Quartz monzonite suite:						
983155A	…	…	…	535	5	870, 1 core
Lac Aigneau enderbite suite:						
994052A	752 ± 19	836	742	544	5	…
991212A	…	…	648	…	…	…
Cpx-diorite and tonalite (CT suite):						
991213A	…	727	…	…	…	…
991103	…	697	…	…	…	…
TTG suite:						
991100A	…	…	…	465	5	550, 1 phenocryst
Lac Maricourt enderbite:						
995254	…	…	719	527	5	…
Cpx-diorite (CT suite):						
991190	…	804	…	…	…	…
Lac Vernon enderbite suite:						
00196B	767 ± 36	732	764	…	…	…
00197A1	864 ± 48	756	911	…	…	…
00196A3	…	…	765	462	3	…

Note. Results of pyroxene thermometry calculated using QUILF (Andersen et al. 1993). Two-feldspar thermometry (Plag/AF) was calculated using SOVCALC2 (Wen and Nekvasil 1994). Reintegrated antiperthites (see text) were plotted on the ternary feldspar diagram (fig. 7), and the temperature approximated through comparison with the 5 kbar solvus, which is in the middle of the pressure range given by Al-in-hornblende barometry. Ba was ignored.

ite cores, some with igneous growth zoning (figs. 3, 5). In addition, the abundance and distribution of epidote among different TT facies conforms to the pattern expected for a minor phase in an igneous differentiation series. Specifically, epidote is absent in diorite, abundant in tonalite (up to 10%, typically 1%–2%), and becomes less abundant in trondhjemite. Collectively, these features constitute a prima facie case for an igneous origin for Minto epidotes (cf. Zen and Hammarstrom 1984; Evans and Vance 1987; Dawes and Evans 1991; Dahlquist 2001). Finally, the absence of epidote in amphibole-rich diorite, and its presence in amphibole-free trondhjemite, are inconsistent with a metamorphic origin through amphibole breakdown.

Metamorphic epidote is present but typically forms discrete, darker-green, Fe-rich rims (table 2) on igneous epidote grains, typically in association with chlorite (fig. 4). Secondary epidote also occurs in sericitized plagioclase. Secondary epidote probably formed during a hydrothermal alteration event, either deuteric or regional in scale, possibly associated with fluid flow along major fractures or shear zones. Euhedral prismatic metamorphic epidote is common in metabasalt, and in felsic plutons affected by Proterozoic orogenesis, and presumably records prograde metamorphism in these cases.

Igneous epidote and allanite from Minto Block TT-GG-CT plutons commonly have scalloped, embayed, or spongy margins where they touch the quartzofeldspathic matrix but faceted faces when armored by biotite or muscovite (figs. 3, 4). These spongy margins do not resemble coronitic metamorphic reaction textures, having a morphology more typical of magmatic resorption (Skjerlie and Johnston 1992). Epidote grains from unmetamorphosed Phanerozoic tonalites show identical textures, generally attributed to magmatic resorption during decompression (Zen and Hammarstrom 1984; Schmidt and Thompson 1996). The stability of liquidus epidote is sensitive to pressure (fig. 11*B*), with a commonly suggested 6–8 kbar limit (Zen and Hammarstrom 1984), although Schmidt and Thompson (1996) concluded that epidote could remain stable to 3 kbar in oxidized magmas. A 6–8 kbar limit is consistent with the barometric estimates for Minto Block rocks and is tentatively adopted here.

Muscovite in Minto Block TT-GG plutons is interpreted to be igneous on the basis of its composition (high FeO^* and TiO_2) and morphology. Muscovite shows textures indicative of partial magmatic resorption (fig. 3*B*), consistent with experimental data indicating that the stability of liquidus muscovite is sensitive to pressure, with a proposed lower limit of 2–4 kbar (Chatterjee and Johannes 1974; Anderson and Rowley 1981). Variations in oxygen and volatile activity may shift its stability to lower or higher pressure conditions, however (Miller et al. 1981; Zen 1988). Despite uncertainty about absolute pressures of muscovite and epidote destabilization, the presence of these partly resorbed igneous phases implies that most Minto Block TT, GG, and CT series magmas originated at depths where epidote and muscovite were stable and then ascended fairly rapidly as crystal slurries or magmas (Brandon et al. 1996).

These observations imply that the dominant mineralogical characteristics of most Minto Block

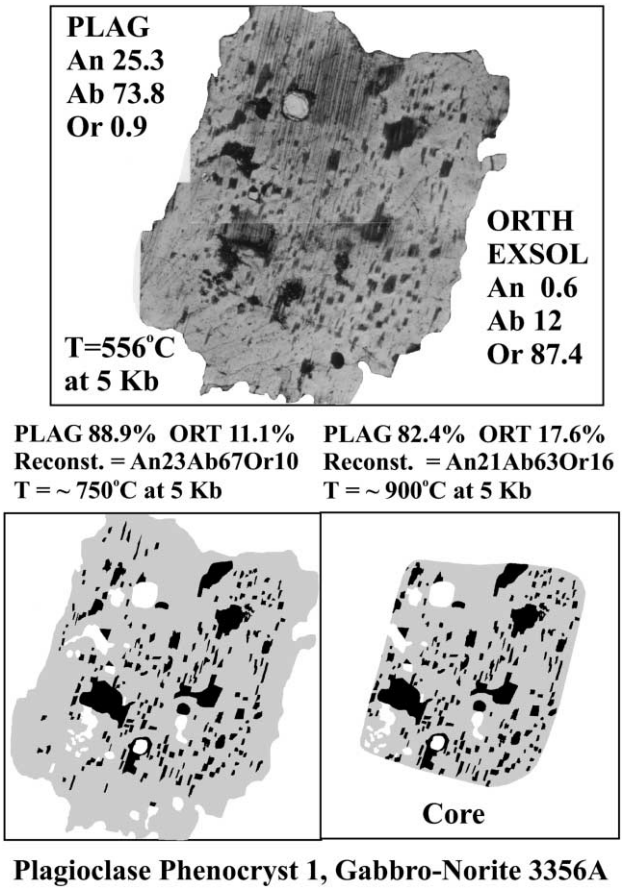

Figure 10. Example of method used to reconstruct antiperthitic plagioclase compositions. *Top*, plagioclase phenocryst from shoshonitic mica diorite 98-3356A. The grain shows a distinct core, with a higher concentration of orthoclase exsolutions than the rim. *Bottom*, results of image analysis (proofed against the thin section) of this grain. Black is orthoclase, gray is plagioclase, and white domains are inclusions.

felsic plutons are not metamorphic in origin, but rather represent stable igneous assemblages. This is consistent with outcrop-scale evidence, indicating that most fabric elements (mafic schlieren, mineral lineation, mineral foliation, preferred mineral orientation) developed before solidification was complete (i.e., these structures and textures formed at the magmatic or submagmatic stage). Furthermore, it is unlikely that the delicate exsolution structures (fig. 6*C*) and widespread magmatic textures and structures (figs. 2–6) could have survived a major amphibolite- to granulite-grade thermal event associated with orogen-scale penetrative deformation and transposition. The preservation of synkinematic magmatic mineralogies and fabrics in most Minto Block plutonic rocks of all domains,

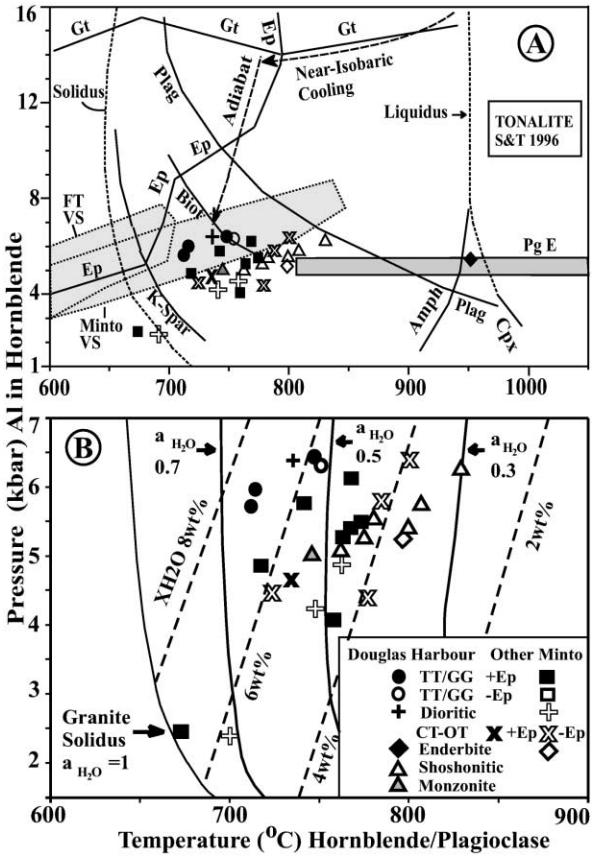

Figure 11. *A*, Pressures calculated using the Schmidt (1992) calibration of the Al-in-hornblende geobarometer plotted against temperatures calculated using the Blundy and Holland (1990) geothermometer, compared to pressure and temperature determinations on supercrustal rocks (*VS*). The Minto VS field is from Percival and Skulski (2000). The field labeled *FT-VS* (Baille-Barrelle et al. 2000) is for amphibolite-grade rocks from the Faribault-Thury complex. Shaded fields labeled *Pg* are the reconstructed feldspar temperatures (this article) applied to rocks of the enderbite (*E*) series. Solid lines show limits of mineral stabilities, while light dashed lines show solidus and liquidus curves for a tonalite investigated by Schmidt and Thompson (1996). *Gt* = garnet, *Ep* = epidote, *Plag* = plagioclase, *Amph* = amphibole, *Biot* = biotite, *K-Spar* = alkali feldspar, *Cpx* = clinopyroxene. The heavy dashed arrows show a possible trajectory for epidote-bearing TTG magmas from the Minto. Adiabatic path taken from Johannes and Holtz (1991). Note that results from the Faribault-Thury complex of the Douglas Harbour domain are offset to higher pressures in comparison to those from other parts of the Minto; that gabbro-norites, a monzonite, and an enderbite (not shown in *B*) from the Troie complex and Qimussinguat complex do not preserve these higher pressures; and that epidote-free TT-GG-CT-OT (*−Ep*) record higher temperatures than epidote-bearing (*+Ep*) variants. *B*, Same data compared to the position of the granitic solidus (Johannes and Holtz 1991) for various water activities and wt% H_2O contents.

with crystallization ages between 2.9 and 2.7 Ga, seems to preclude the possibility that the NNW structural grain (D2) is due to an overprinting, subsolidus, tectonometamorphic event involving complete recrystallization and transposition.

This is not to say that there is no plastic deformation recorded in these rocks. On the contrary, most show some degree of subsolidus strain, which becomes more intense in the shear zones bounding major units, or in zones where L-tectonites are developed. However, the common dissected, high-energy feldspar-feldspar grain boundaries and rotational subgrains (fig. 3*F*) suggest high temperature recrystallization by fast grain boundary migration (Tullis and Yund 1985; Lafrance et al. 1996; Vigneresse et al. 1996; Rosenberg 2001). This contrasts with the straight, well-equilibriated feldspar grains (120° triple junctions) in adjacent metabasalt, which are typical of prograde metamorphic recrystallization (Kretz 1966; Vernon 1999). The fact that quartz appears to have behaved more plastically than feldspar in the felsic plutons also suggests high (>900°C) temperature deformation (Dell'Angelo and Tullis 1996). Preservation of igneous textures in epidote during deformation may be due to its relative rigidity (Kruse and Stünitz 1999) or to the presence of a lubricating melt. Muscovite is weaker than epidote, and its primary textures are less commonly preserved as a consequence. Since submagmatic plastic overprints are generally parallel with the synmagmatic fabrics (Madore et al. 1999; Bédard et al. 2003), it seems more probable that plastic deformation in the felsic plutonic rocks was a continuation of synmagmatic deformation through the rheological locking point into the sub-subsolidus (Hibbard 1987; Paterson et al. 1989; Pavlis 1996; Vigneresse et al. 1996). Although explaining the causes of this plastic deformation is beyond the scope of this article, Bédard et al. (2003) propose that much of it results from partial convective crustal overturn (Bouhallier et al. 1995; Collins et al. 1998) driven by subsidence of dense greenstones + solidified felsic intrusions, into buoyant, incompletely solidified felsic magmas.

Metamorphism of Supercrustal Belts: Synkinematic Pluton-Driven Contact Metamorphism or Regional Orogenesis? Different causes for metamorphism of the supercrustal rocks in the Minto can be envisaged.

1. Percival and Skulski (2000) proposed that crustal thickening caused by obduction of the Tikkerutuk arc caused metamorphism of the supercrustal rocks to amphibolite and granulite grade in the central and eastern Minto Block. However, the general absence of shallowly dipping fabrics (Per-

cival and Card 1994; Leclair et al. 2001; Parent et al. 2002) seems inconsistent with a major terrane obduction event. In addition, this model cannot account for similar metamorphism in the eastern Minto Block, since this crust-thickening event is supposedly restricted to the western Minto Block (Percival and Skulski 2000). Furthermore, if the western Minto Block was affected by a major crust-thickening/exhumation event, then why do eastern and western Minto rocks show such remarkable petrographic and structural similarities and yield such similar Al-in-hornblende pressures (all 4–6 kbar; Percival et al. 1992; Percival and Skulski 2000; this article)? Finally, the weight of evidence (see above) favors an igneous origin for most minerals and a synmagmatic origin for much of the fabric development in Minto Block plutons. It is difficult to conceive of an orogen-scale tectonometamorphic event that would only affect the narrow supercrustal belts and not the plutons in which they are embedded.

2. Metamorphism in the supercrustal rocks may record an older (pre-2.81 Ga) regional Barrovian event, as inferred by Percival and Skulski (2000) for the Qalluviartuuq area. This model cannot explain metamorphism of post-2.81 Ga supercrustal belts, however.

3. Metamorphism in supercrustal rocks could be the result of pluton emplacement and thermal and/or chemical equilibration with surrounding intrusions (Ayres 1978; Frost et al. 1989; Bégin and Pattison 1994; Kamber and Biino 1995; Rollinson and Blenkinsop 1995). The ascent of plutons is known to be an efficient vector for heat transfer (Barton and Hanson 1989; Vernon et al. 1993); and previous studies (Jolly 1974; Ayres 1978; Easton 2000; Barros et al. 2001) concluded that contact metamorphic aureoles around Archean granitoids can extend several kilometers from their contacts. In general, amphibolite-grade belts in the Minto are associated with TT-GG plutons, while granulite-grade belts are associated with E-CT-OT series plutons—a dichotomy that suggests a genetic link. Bégin and Pattison (1994) noted an even finer-scale correlation, with the highest temperature assemblages in granulite-grade metasediments being associated with more mafic intrusions, and lower temperature assemblages being associated with more felsic plutons. Either (*a*) the plutonic-supercrustal assemblages were metamorphosed together, with plutons recording conditions similar to the embedded supercrustal slivers; or (*b*) mineral assemblages in the narrow supercrustal slivers of the Minto Block reflect thermal and chemical equilibration with the larger "system" represented by surrounding plutons. The textural evidence and discussion presented above imply that mineral assemblages and fabrics in Minto Block plutonic rocks are dominantly igneous, which is inconsistent with (*a*). Conversely, the spatial associations and development of pyroxene-bearing reaction rims on amphibolitic xenoliths in enderbitic plutons (fig. 6*B*; Percival et al. 1992) support (*b*). Therefore, the evidence strongly supports a pluton-driven process, where mineral assemblages in supercrustal rocks mainly reflect equilibration with adjacent plutons. Thus, amphibolites formed by wet, cool, metamorphism induced by TT-GG series intrusions, while granulites formed through dry, hot metamorphism induced by H_2O-undersaturated E-CT-OT series intrusions. Rare exceptions to this pattern could reflect shuffling by late deformation events (D3–D5), emplacement of minor pulses of the other magma types along favorable structures, or complexities inherent to a prolonged intrusion history (e.g., Wells 1980).

It is useful to consider how midcrustal temperatures might evolve during a craton-forming magmatic event. A significant geochronological database now exists for the Minto Block, through the work of John Percival, Tom Skulski, Jim Mortensen, and Jean David. These data indicate that most of the Minto crust formed between 2.9 and 2.7 Ga, with peak activity around 2.74–2.72 Ga. How would such an immense volume of newly emplaced magma cool? The lateral extent of coeval plutonism (many hundreds of kilometers) precludes heat loss from the sides. Supercrustal rocks are only a small fraction (~5%–15%) of the crustal volume, so could not have played a significant role in absorbing magmatic heat. Consequently, only heat loss through the roof by exchanges with the hydrosphere should be significant. Studies of fast-spreading ocean ridges provide insight into the behavior of such systems (Peters et al. 1991; Dilek et al. 2000), which are characterized by continuous inputs of magma from below that buffer deep-crustal temperatures at or near the solidus. Heat loss from above, however, is limited due to the development of thermally opaque boundary layers in the roof zones of high-level magma chambers and because it is difficult for water to penetrate hot, mushy crust. A similar situation for the nascent lower/middle Archean crust might be inferred.

The absence of chilled margins, or of textural evidence in Minto plutons for prograde greenschist to amphibolite reactions, together with the common 2.705–2.62 Ga titanite/monazite ages (Percival and Skulski 2000), suggest that most pre-2.7 Ga intrusions in the Minto were not separated by sig-

nificant cooling events. This implies that Minto plutons cooled very slowly, so I infer that, during craton formation (2.9–2.7 Ga), the high magma flux (e.g., Wells 1980); ongoing underplating by komatiitic and basaltic magmatism (e.g., Fyfe 1992); emplacement of voluminous, hot (1000°–1050°C), enderbite-suite magmas; the absence of an effective sink for advected heat (see above); and the higher content of radioactive nucleides in the Archean (Kramers et al. 2001); would have acted together to keep the middle crust at near-solidus temperatures (650°–850°C) for extended periods. Since supercrustal rocks record temperatures slightly cooler than adjacent plutons (fig. 11*B*), anatexis of metapelites may have buffered temperatures in supercrustal belts (Hodges et al. 1988), with inputs of heat energy from adjoining plutons converting solid into liquid, rather than raising temperatures. Estimates of monazite closure temperatures are controversial, but a titanite closure temperature of 650°–700°C is widely accepted (Möller et al. 2000). Assuming a 700°C titanite closure temperature, the time between the thermal maximum associated with peak Leaf River Suite magmatism at 2.725 Ga and the 2.7–2.65 Ga titanite ages implies moderate cooling rates between 8° and 3°C/Ma if an average liquidus temperature of 900°C is assumed.

Conclusions

Most tonalitic, granodioritic, and enderbitic intrusions in the Minto Block record near-solidus equilibration temperatures, and many retain igneous textures. Mineral-chemical signatures are dominantly igneous. Resorption structures in igneous epidote and muscovite imply ascent from depth as crystal-charged magmas. Outcrop-scale structures suggest largely synmagmatic deformation, with strain continuing through the rheological locking point into the subsolidus. This observation seems to be inconsistent with development of fabrics as a result of a late regional tectonometamorphic overprint. Amphibolite-grade supercrustal rocks are associated with tonalitic or granitic plutons, while granulite-grade belts are associated with enderbitic or pyroxene-tonalite series plutons. This dichotomy suggests that mineral assemblages in supercrustal belts reflect equilibration with adjacent plutons, rather than differences in grade linked to collisional orogenesis. Supercrustal rocks are indeed sensitive recorders of pressure-temperature conditions, but the Minto crust is essentially plutonic, and the ascent and cooling history of these plutons probably controlled the temperatures of supercrustal slivers.

ACKNOWLEDGMENTS

This study was made possible through the logistical assistance and hospitality of the Ministère des Ressources Naturelles du Québec. I particularly wish to thank A. Berclaz, A.-M. Cadieux, C. Gosselin, Y. Larbi, A. Leclair, L. Madore, C. Maurice, M. Parent, and M. Simard. Valuable comments and reviews were provided by R. Frost, J. Percival, L. Corriveau, T. Rushmer, and L. Madore. H. Nekvasil and D. Lindsley provided software. L. Dubé and M. Boutin helped with the figures. M. Choquette assisted with the microprobe. This is Geological Survey of Canada contribution 2001154 and Ministère des Ressources Naturelles du Québec contribution 2001-5130-20.

REFERENCES CITED

Andersen, D. J.; Lindsley, D. H.; and Davidson, P. M. 1993. QUILF: a Pascal program to assess equilibria among Fe-Mg-Mn-Ti oxides, pyroxenes, olivine, and quartz. Comput. Geosci. 19:1333–1350.

Anderson, J. L., and Rowley, M. C. 1981. Synkinematic intrusion of two-mica and associated metaluminous granitoids, Whipple Mountains, California. Can. Mineral. 19:83–101.

Anderson, J. L., and Smith, D. R. 1995. The effects of temperature and f_{O2} on the Al-in-hornblende barometer. Am. Mineral. 80:549–559.

Ayres, L. D. 1978. Metamorphism in the Superior Province of northwestern Ontario and its relationship to crustal development. *In* Fraser, J. A., and Heywood, W. W., eds. Metamorphism in the Canadian Shield. Geol. Surv. Can. Pap. 78-10, p. 25–36.

Baille-Barrelle, B.; Goulet, N.; and Madore, L. 2000. Un "metamorphic core complex" dans le domaine de Douglas Harbour, sous-Province de Minto, (Province du Supérieur)? *In* Leclair, A., ed. Projet de Cartographie du Grand Nord, Rapport d'Atelier, Avril 5–6, 2000, Charlesbourg, Québec. Minist. Ress. Nat. Que., Rapp. 2, p. 1–4.

Barros, C. E. M.; Barbey, P.; and Boullier, A. M. 2001. Role of magma pressure, tectonic stress and crystallization progress in the emplacement of syntectonic granites: the A-type Estrela Granite Complex (Carajas Mineral Province, Brazil). Tectonophysics 343:93–109.

Barton, M. D., and Hanson, R. B. 1989. Magmatism and the development of low-pressure metamorphic belts: Implications from the western United States and thermal modeling. Geol. Soc. Am. Bull. 101:1051–1065.

Bédard, J. H.; Brouillette, P.; Madore, L.; and Berclaz, A. 2003. Archaean cratonization and deformation in the

northern Superior Province, Canada: an evaluation of plate tectonic versus vertical tectonic models. Precambrian Res., in press.

Bédard, J. H.; Madore, L.; and Brouillette, P. 2001. Polybaric syn-kinematic tonalite-trondhjemite plutonism in the Archaean Minto Block, Superior Province. Geol. Assoc. Can./Mineral. Assoc. Can. Progr. Abstr. 33, p. A18.

Bégin, N. J., and Pattison, D. R. M. 1994. Metamorphic evolution of granulites in the Minto Block, northern Québec: extraction of peak P-T conditions taking account of late Fe-Mg exchange. J. Metamorph. Geol. 12:411–428.

Berclaz, A.; Cadieux, A.-M.; Sharma, K. N. M.; Parent, M.; and Leclair, A. 2001. Géologie de la région du Lac Aigneau (SNRC 24E et 24F04). Minist. Ress. Nat. Que., Rapp. Geol. RG 2001-01, 49 p.

Blundy, J. D., and Holland, T. J. B. 1990. Calcic amphibole equilibria and a new amphibole-plagioclase geothermometer. Contrib. Mineral. Petrol. 104:208–224.

Bouhallier, H.; Chardon, D.; and Choukroune, P. 1995. Strain patterns in Archaean dome-and-basin structures: the Dharwar craton (Karnataka, South India). Earth Planet. Sci. Lett. 135:57–75.

Brandon, A. D.; Creaser, R. A.; and Chacko, T. 1996. Constraints on rates of granitic magma transport from epidote dissolution kinetics. Science 271:1845–1848.

Brey, G. P., and Köhler, T. 1990. Geothermobarometry in four-phase lherzolites. II. New thermobarometers, and practical assessment of existing thermobarometers. J. Petrol. 31:1353–1378.

Burbank, D. W. 2002. Rates of erosion and their implications for exhumation. Min. Mag. 66:25–52.

Cadieux, A.-M.; Berclaz, A.; Labbé, J.-Y.; Lacoste, P.; David, J.; and Sharma, K. N. M. 2002. Géologie de la région du Lac Pélican (SNRC 34P). Minist. Ress. Nat. Que., Rapp. Geol. RG 2002-02, 49 p.

Card, K. D. 1990. A review of the Superior Province of the Canadian Shield, a product of Archean accretion. Precambrian Res. 48:99–156.

Card, K. D., and Ciesielski, A. 1986. Subdivisions of the Superior Province of the Canadian Shield. Geosci. Can. 13:5–13.

Chatterjee, N. D., and Johannes, W. 1974. Thermal stability and standard thermodynamic properties of synthetic 2M1 muscovite, $KAl_2AlSi_3O_{10}(OH)_2$. Contrib. Mineral. Petrol. 49:89–114.

Collins, W. J.; Van Kranendonk, M. J.; and Teyssier, C. 1998. Partial convective overturn of Archaean crust in the east Pilbara Craton, Western Australia: driving mechanisms and tectonic implications. J. Struct. Geol. 20:1405–1424.

Cumbest, R. J.; Drury, M. R.; van Roermund, H. L. M.; and Simpson, C. 1989. Dynamic recrystallization and chemical evolution of clinoamphibole from Senja, Norway. Contrib. Mineral. Petrol. 101:339–349.

Dahlquist, J. A. 2001. Low-pressure emplacement of epidote-bearing metaluminous granitoids in the Sierre de Chepes (Famatinian Orogen, Argentina) and relationships with the magma source. Rev. Geol. Chile 28:147–161.

Dawes, R. L., and Evans, B. W. 1991. Mineralogy and geothermobarometry of magmatic epidote-bearing dikes, Front Range, Colorado. Geol. Soc. Am. Bull. 103:1017–1031.

Dell'Angelo, L. N., and Tullis, J. 1996. Textural and mechanical evolution with progressive strain in experimentally deformed aplite. Tectonophysics 256:57–82.

Dilek, Y.; Moores, E. M.; Elthon, D.; and Nicolas, A. 2000. Ophiolites and oceanic crust: new insights from field studies and ocean drilling program. Geol. Soc. Am. Spec. Publ. 349, 466 p.

Easton, R. M. 2000. Metamorphism of the Canadian Shield, Ontario, Canada. I. The Superior Province. Can. Mineral. 38:287–317.

Evans, B. W., and Vance, J. A. 1987. Epidote phenocrysts in dacitic dikes, Boulder County, Colorado. Contrib. Mineral. Petrol. 96:178–185.

Frost, B. R.; Frost, C. D.; Hulsebosch, T. P.; and Swapp, S. M. 2000. Origin of the charnockites of the Louis Lake Batholith, Wind River Range, Wyoming. J. Petrol. 41:1759–1776.

Frost, B. R.; Frost, C. D.; and Touret, J. L. R. 1989. Magmas as a source of heat and fluids in granulite metamorphism. *In* Bridgewater, D., ed. Fluid movements: element transport and the composition of the deep crust. Dordrecht, Kluwer, p. 1–18.

Fyfe, W. S. 1992. Magma underplating of continental crust. J. Volc. Geotherm. Res. 50:44–40.

Gapais, D. 1989. Shear structures within deformed granites: mechanical and thermal indicators. Geology 17: 1144–1177.

Gosselin, C., and Simard, M. 2001. Géologie de la région des lacs des Loups Marins (SNRC 34A). Minist. Ress. Nat. Que. RG 2001-10 (accompanies map SI-34A-C2G-01K, scale 1 : 250,000), 42 p.

Hammarstrom, J. M., and Zen, E.-A. 1986. Aluminum in hornblende: an empirical igneous geobarometer. Am. Mineral. 71:1297–1313.

Hibbard, M. J. 1987. Deformation of incompletely crystallized magma systems: granitic gneisses and their tectonic implications. J. Geol. 95:543–561.

Hibbard, M. J., and Watters, R. J. 1985. Fracturing and diking in incompletely crystallized granitic plutons. Lithos 18:1–12.

Hodges, K. V.; Le Fort, P.; and Pêcher, A. 1988. Possible thermal buffering by crustal anatexis in collisional orogens: thermobarometric evidence from the Nepalese Himalaya. Geology 16:707–710.

Hogan, J. P. 1996. Insights from igneous reaction space: A holistic approach to granite crystallisation. Trans. R. Soc. Edinb. Earth Sci. 87:147–157.

Johannes, W., and Holtz, F. 1991. Formation and ascent of granitic magmas. Geol. Rundsch. 80:225–231.

Johnson, M. C., and Rutherford, M. J. 1989. Experimental calibration of the aluminum-in-hornblende geobarometer with application to Long Valley Caldera (California) volcanic rocks. Geology 17:837–841.

Jolly, W. T. 1974. Regional metamorphic zonation as an

aid in study of Archean terrains: Abitibi region, Ontario. Can. Mineral. 12:499–508.
Kamber, B. S., and Biino, G. G. 1995. The evolution of high T–low pressure granulites in the Northern Marginal Zone sensu stricto, Limpopo Belt, Zimbabwe: the case for petrography. Schweiz. Mineral. Petrol. Mitt. 75:427–454.
Kilpatrick, J. A., and Ellis, D. J. 1992. C-type magmas: igneous charnockites and their extrusive equivalents. Trans. R. Soc. Edinb. Earth Sci. 83:155–164.
Kramers, J. D.; Kreissig, K.; and Jones, M. Q. W. 2001. Crustal heat production and style of metamorphism: a comparison between two Archean high grade provinces in the Limpopo Belt, southern Africa. Precambrian Res. 112:149–163.
Kretz, R. 1966. Interpretation of the shape of mineral grains in metamorphic rocks. J. Petrol. 7:68–94.
Kriegsman, L. M. 2001. Partial melting, partial melt extraction and partial back reaction in anatectic migmatites. Lithos 56:75–96.
Kruse, R., and Stünitz, H. 1999. Deformation mechanisms and phase distribution in mafic high-temperature mylonites from the Jotun Nappe, southern Norway. Tectonophysics 303:223–249.
Lafrance, B.; John, B. E.; and Scoates, J. S. 1996. Syn-emplacement recrystallization and deformation microstructures in the Poe Mountain anorthosite, Wyoming. Contrib. Mineral. Petrol. 122:431–440.
Leclair, A.; Parent, M.; David, J.; Dion, D.-J.; and Sharma, K. N. M. 2001. Géologie de la région du lac La Potherie (SNRC 34I). Minist. Ress. Nat. Que., Rapp. Geol. RG 2001-12, 46 p.
Lin, S. F.; Percival, J. A.; and Skulski, T. 1996. Structural constraints on the tectonic evolution of a late Archean greenstone belt in the northeastern Superior Province, northern Quebec (Canada). Tectonophysics 265: 151–167.
Madore, L.; Bandyayera, D.; Bédard, J. H.; Brouillette, P.; Sharma, K. N. M.; Beaumier, M.; and David, J. 1999. Géologie de la région du Lac Peters (SNRC 24M). Minist. Ress. Nat. Que., Rapp. Geol. RG 99-07, 41 p.
Madore, L., and Larbi, Y. 2000. Géologie de la région de la Rivière Arnaud (SNRC 25D) et des régions littorales adjacentes (SNRC 25C, 25E et 25F). Min. Ress. Nat. Que., Rapp. Geol. RG 2000-05, 37 p.
Madore, L.; Larbi, Y.; Labbé, J.-Y.; Lacoste, P.; David, J.; Brousseau, K.; and Hocq, M. 2001. Géologie de la région du lac Klotz (SNRC 35A) et du cratère du Nouveau Québec (1/2 sud de SNRC 35H). Minist. Ress. Nat. Que., Rapp. Geol. 2000-09, 44 p.
Miller, C. F.; Stoddard, D. F.; Bradfish, L. J.; and Dollase, W. A. 1981. Composition of plutonic muscovite: genetic implications. Can. Mineral. 19:25–34.
Möller, A.; Mezger, K.; and Schenk, V. 2000. U-Pb dating of metamorphic minerals: Pan-African metamorphism and prolonged slow cooling of high pressure granulites in Tanzania, East Africa. Precambrian Res. 104:123–146.
Parent, M.; Leclair, A.; David, J.; Sharma, K. N. M.; and Lacoste, P. 2002. Géologie de la région du lac Vernon (SNRC 34J). Minist. Ress. Nat., Que., Rapp. Geol. RG 2001-11, 40 p.
Paterson, S. R.; Vernon, R. H.; and Tobisch, O. T. 1989. A review of criteria for the identification of magmatic and tectonic foliations in granitoids. J. Struct. Geol. 11:349–363.
Pavlis, T. L. 1996. Fabric development in syn-tectonic intrusive sheets as a consequence of melt-dominated flow and thermal softening of the crust. Tectonophysics 253:1–31.
Percival, J. A., and Berman, R. G. 1996. Minto block: metamorphic-plutonic hinterland in northeastern Superior Province. Geol. Assoc. Can./Mineral. Assoc. Can. Prog. Abstr. 21, p. A74.
Percival, J. A., and Card, K. D. 1994. Geology, Lac Minto-Rivière aux Feuilles, Québec. Geol. Surv. Can. Map 1854A, scale 1 : 500,000.
Percival, J. A.; Card, K. D.; and Mortensen, J. K. 1993. Archean unconformity in the Vizien greenstone belt, Ungava Peninsula, Quebec. Geol. Surv. Can., Curr. Res. 1993-1C, p. 319–328.
Percival, J. A., and Mortensen, J. K. 2002. Water-deficient calc-alkaline plutonic rocks of the northeastern Superior Province, Canada: significance of charnockitic magmatism. J. Petrol. 43:1617–1650.
Percival, J. A.; Mortensen, J. K.; Stern, R. A.; Card, K. D.; and Bégin, N. J. 1992. Giant granulite terranes of northeastern Superior Province: the Ashuanipi Complex and Minto Block. Can. J. Earth Sci. 29:2287–2308.
Percival, J. A., and Skulski, T. 2000. Tectonothermal evolution of the northern Minto block, Superior Province, Quebec, Canada. Can. Mineral. 38:345–378.
Percival, J. A.; Skulski, T.; Card, K. D.; and Lin, S. 1995. Geology of the Rivière Kogaluc–Lac Qalluviartuuq region (parts of 34J and 34O), Quebec. Geol. Surv. Can., Open File Map 3112, scale 1 : 250,000.
Percival, J. A.; Skulski, T.; and Nadeau, L. 1997. Granite-greenstone terranes of the northern Minto block, northeastern Quebec: Pelican-Nantais, Faribault-Leridon, and Duquet belts. Geol. Surv. Can., Curr. Res. 1997C, p. 211–221.
Percival, J. A.; Stern, R. A.; and Skulski, T. 2001. Crustal growth through successive arc magmatism, northeastern Superior Province, Canada. Precambrian Res. 109:203–238.
Percival, J. A.; Stern, R. A.; Skulski, T.; Card, K. D.; Mortensen, J. K.; and Bégin, N. J. 1994. Minto Block, Superior Province: missing link in deciphering assembly of the Craton at 2.7 Ga. Geology 22:839–842.
Peters, T.; Nicolas, A.; and Coleman, R. G. 1991. Ophiolite genesis and evolution of the oceanic lithosphere. Dordrecht, Kluwer, 903 p.
Piccoli, P.; Candela, P.; and Rivers, M. 2000. Interpreting magmatic processes from accessory phases: titanite—a small-scale recorder of large-scale processes. Trans. R. Soc. Edinb. Earth Sci. 91:257–267.
Pitcher, W. S. 1991. Synplutonic dykes and mafic enclaves. *In* Didier, J., and Barbarin, B., eds. Enclaves and granite petrology. Amsterdam, Elsevier, p. 383–391.

Raase, P. 1998. Feldspar thermometry: a valuable tool for deciphering the thermal history of granulite-facies rocks, as illustrated with metapelites from Sri Lanka. Can. Mineral. 36:67–86.

Rapp, R. P., and Watson, E. B. 1986. Monazite solubility and dissolution kinetics implications for the thorium and light rare earth chemistry of felsic magmas. Contrib. Mineral. Petrol. 94:304–316.

Rollinson, H. R., and Blenkinsop, T. 1995. The magmatic, metamorphic, and tectonic evolution of the Northern Marginal Zone of the Limpopo Belt in Zimbabwe. J. Geol. Soc. Lond. 152:65–75.

Rosenberg, C. L. 2001. Deformation of partially molten granite: a review and comparison of experimental and natural case studies. Int. J. Earth Sci. (Geol. Rundsch.) 90:60–76.

Sawyer, E. W. 2000. Grain-scale and outcrop-scale distribution and movement of melt in a crystallising granite. Trans. R. Soc. Edinb. Earth Sci. 91:73–85.

Schmidt, M. W. 1992. Amphibole composition in tonalite as a function of pressure: an experimental calibration of the Al-in-hornblende barometer. Contrib. Mineral. Petrol. 110:304–310.

Schmidt, M. W., and Thompson, A. B. 1996. Epidote in calc-alkaline magmas: an experimental study of stability, phase relationships, and the role of epidote in magmatic evolution. Am. Mineral. 81:462–474.

Simard, M.; Gosselin, C.; and David, J. 2001. Géologie de la région de Maricourt (SNRC 24D). Min. Ress. Nat. Que., Rapp. Geol. RG 2000-07, 50 p. (accompanies map SI-24D-C2G-00K, scale 1 : 250,000).

Skjerlie, K. P., and Johnston, A. D. 1992. Vapor-absent melting at 10-kbar of a biotite- and amphibole-bearing tonalitic gneiss: implications for the generation of A-type granites. Geology 20:263–266.

Skulski, T., and Percival, J. A. 1996. Allochthonous 2.78 Ga oceanic plateau slivers in a 2.72 Ga continental arc sequence: vizien greenstone belt, northeastern Superior province, Canada. Lithos 37:163–179.

Skulski, T.; Percival, J. A.; and Stern, R. A. 1994. Oceanic allochthons in an Archean continental margin sequence, vizien greenstone belt, northern Quebec. Geol. Surv. Can. Curr. Res. 1994-C, p. 311–320.

———. 1996. Archean crustal evolution in the central Minto block, northern Quebec. *In* Radiogenic Age and Isotopic Studies Report 9. Ottawa, Ontario, Geol. Surv. Can., Curr. Res. 1995-F, p. 17–31

Speer, J. A. 1984. Micas in igneous rocks. Mineral. Soc. Am. Rev. Mineral. 13:299–356.

Stern, R. A., Percival, J. A., and Mortensen, J. K. 1994. Geochemical evolution of the Minto Block: a 2.7 Ga continental magmatic arc built on the Superior protocraton. Precambrian Res. 65:115–153.

Stevenson, I. M. 1968. A geological reconnaissance of the Leaf River map-area, New Quebec and Northwest Territories. Geol. Surv. Can. Mem. 356, 112 p.

St.-Onge, M. R., and Ijewliw, O. J. 1996. Mineral corona formation during high-P retrogression of granulitic rocks, Ungava Orogen, Canada. J. Petrol. 37:553–582.

Stünitz, H., and Tullis, J. 2001. Weakening and strain localization produced by syn-deformational reaction of plagioclase. Int. J. Earth Sci. (Geol. Rundsch.) 90: 136–148.

Thompson, A. B., and Ellis, D. J. 1994. CaO + MgO + Al_2O_3 + SiO_2 + H_2O to 35 kb: amphibole, talc, and zoisite dehydration and melting reactions in the silica-excess part of the system and their possible significance in subduction zones, amphibolite melting, and magma fractionation. Am. J. Sci. 294:229–1289.

Tindle, A. G., and Webb, P. C. 1994. PROBE-AMPH—a spreadsheet program to classify microprobe-derived amphibole analyses. Comput. Geosci. 20:1201–1228.

Tullis, T., and Yund, R. A. 1985. Dynamic recrystallization of feldspar: a mechanism of ductile shear zone formation. Geology 13:238–241.

Vernon, R. H. 1999. Quartz and feldspar microstructures in metamorphic rocks. Can. Mineral. 37:513–524.

———. 2000. Review of microstructural evidence of magmatic and solid-state flow. Electr. Geosci. 5.

Vernon, R. H.; Collins, W. J.; and Paterson, S. R. 1993. Pre-foliation metamorphism in low-pressure/high-temperature terrains. Tectonophysics 219:241–256.

Vigneresse, J. L.; Barbey, P.; and Cuney, M. 1996. Rheological transitions during partial melting and crystallization with application to felsic magma segregation and transfer. J. Petrol. 37:1579–1600.

Wells, P. R. A. 1980. Thermal models for the magmatic accretion and subsequent metamorphism of continental crust. Earth Planet. Sci. Lett. 46:253–265.

Wen, S., and Nekvasil, H. 1994. SOLVCALC: an interactive graphics program package for calculating the ternary feldspar solvus and for two-feldspar geothermometry. Comput. Geosci. 20:1025–1040.

Wolf, M. B., and London, D. 1995. Incongruent dissolution of REE- and Sr-rich apatite in peraluminous granitic liquids: differential apatite, monazite, and xenotime solubilities during anatexis. Am. Mineral. 80: 765–775.

Zen, E.-A. 1986. Aluminium enrichment in silicate melts by fractional crystallization: some mineralogical and petrographic constraints. J. Petrol. 27:1095–1117.

———. 1988. Phase relations of peraluminous granitic rocks and their petrogenetic implications. Annu. Rev. Earth Planet. Sci. 16:21–51.

Zen, E.-A., and Hammarstrom, J. M. 1984. Magmatic epidote and its petrological significance. Geology 12: 515–518.